Hindawi
Journal of Food Biochemistry
Volume 2024, Article ID 9945178, 23 pages
https://doi.org/10.1155/2024/9945178

Research Article

Quercetin Promotes Apoptosis of Gastric Cancer Cells through the EGFR-ERK Signaling Pathway

Yali Liu,[1,2] **Yan Li**,[2] **Yanjun Jiang**,[3] **Xin Zheng**,[2] **Tianming Wang**,[4] **Jing Li**,[2] **Biyun Zhang**,[5] **Jiarui Zhu**,[2] **Xintong Wei**,[6] **Ruihua Huang**,[6] **Yong Zhang**,[1] **and Qiaoying Jin**[2]

[1]*College of Veterinary Medicine, Gansu Agricultural University, Lanzhou, China*
[2]*The Second Hospital & Clinical Medical School, Lanzhou University, Lanzhou, China*
[3]*Gansu Jiantou Technology Research and Development Co., Ltd., Lanzhou, China*
[4]*No. 92 Middle School of Lanzhou, Lanzhou, China*
[5]*Tianshui Fourth People's Hospital, Tianshui, China*
[6]*The Second Clinical Medical College, Lanzhou University, Lanzhou, China*

Correspondence should be addressed to Yong Zhang; zhangyong@gsau.edu.cn and Qiaoying Jin; jinqy09@163.com

Received 5 December 2023; Revised 7 January 2024; Accepted 30 January 2024; Published 13 February 2024

Academic Editor: Ignazio Restivo

Previous studies have shown that various active components of licorice have anticancer effects. However, few studies have investigated the mechanism of action of licorice in gastric cancer. The effect of active compounds in licorice on the biological activity of gastric cancer cells was investigated in vitro (MKN-45 cells). Network pharmacology and molecular docking were used to predict the potential targets of licorice against gastric cancer and verify the binding stability of target proteins to compounds. In addition, the anticancer effect of licorice was assessed using a mouse model of gastric cancer. The licorice-active component (quercetin) effectively inhibited proliferation, caused cell cycle arrest, and promoted apoptosis in MKN-45 cells, accompanied by increased Cyt-C, decreased BCL-2, and decreased mitochondrial membrane potential and mitochondrial damage. Further research showed that quercetin targeted EGFR, blocked the ERK signaling pathway, and downregulated PTGS2. In the in vivo experiment, quercetin treatment resulted in reduced tumor volume, decreased Ki67 and BCL-2 expression in tumor tissue, increased caspase 3 and BAX levels, and induced mitochondrial damage.

1. Introduction

According to a report by the International Agency for Research on Cancer [1], the number of new cases and deaths due to gastric cancer ranked fifth and fourth among malignant tumors in 2020, with 1,090,000 and 770,000 cases, respectively. Gastric cancer is a malignant tumor that seriously affects human health.

With the continuous improvement and progression of medical technology, molecular-targeted drugs (MTDs) have become the main force of tumor treatment. MTD is an immunotherapy; when it enters the body, it selectively binds to its target and exerts an antitumor effect without affecting normal cells. MTD includes monoclonal antibody drugs and natural small-molecule inhibitors. In recent years, monoclonal antibody drugs have achieved satisfactory clinical efficacy in the treatment of various human tumors. However, years of research and clinical application have shown that this technology still has some unavoidable defects, such as nonspecific binding between antibodies and normal tissues, poor penetration of drugs into tumors, rejection of heterologous antibodies by the human body, drug resistance, and high costs.

In recent years, natural small-molecule inhibitors from TCM have shown a better antitumor effects in a variety of human tumors, including oral squamous carcinoma, cervical cancer, cervical cancer, and osteosarcoma [2–6]. Compared to monoclonal antibody drugs, natural antitumor small-molecule inhibitors have unique advantages. These advantages include a molecular weight of less than 1000 Da,

better cell permeability, a faster diffusion rate in the tumor microenvironment, and entering the brain tissue to treat brain tumors with greater ease. In addition, small-molecule inhibitors have a short half-life, allowing them to be administered intermittently to balance the risk of side-effects [7]. These drugs are also mature in terms of production technology, dosage form design, drug delivery mode, and mass manufacturing and expansion is feasible for them. Therefore, the development of novel natural small-molecule inhibitors is an effective way to treat gastric cancer.

Licorice is one of the most common Chinese herbs, with effects such as invigorating the spleen, replenishing qi, moistening the lungs, eliminating phlegm, clearing heat, and exerting antioxidant effects. In recent years, the antitumor effects of licorice have been reported. For example, the inhibitory effect of licorice acid on gastric cancer cells was accomplished by downregulating the PI3K/AKT pathway, thereby inducing cell cycle arrest and apoptosis [8]. Liquiritin, a flavone compound derived from licorice, could increase the area under the curve and maximum plasma concentration of antitumor drugs [9]. Licochalcone A, a chalcone isolated from licorice root, interfered with the mitogen-activated protein kinase (MAPK) signaling pathway, induced oxidative stress, initiated reactive oxygen species (ROS) generation, and triggered apoptosis in gastric cancer cells [10]. Isoliquiritigenin, another licorice-derived flavonoid, inhibited the migration, invasion, and proliferation of human gastric cancer cells (MKN-28) by inducing apoptosis and autophagy [11].

The antitumor effects of traditional Chinese medicine (TCM) involve multicomponent, multitarget, and multisignaling pathways. To systematically investigate the mechanism of action of licorice against gastric cancer and evaluate its therapeutic effect, we evaluated the effects of licorice on proliferation capacity, cell morphology, apoptosis rate, mitochondrial morphology, and key signaling pathways in gastric cancer cells in vitro and in vivo to identify an effective natural small-molecule inhibitor to treat gastric cancer.

2. Materials and Methods

2.1. Cell Culture and CCK-8 Assay. The human gastric cancer cell line MKN-45 was obtained from Cuiying Biomedical Research Center, the Second Hospital and Clinical Medical School, Lanzhou University. The cells were cultured in Dulbecco's modified Eagle medium containing 10% fetal bovine serum in an incubator at 37°C with 5% CO_2. The cells were divided into negative control (no dosing), treatment with the main active components of licorice, and positive drug (lapatiunib) treatment groups. Quercetin (Sigma-Aldrich, Q4951), isorhamnetin (Cayman Chemical, 16496), licochalcone A (Sigma-Aldrich, 435800), naringenin (Sigma-Aldrich, 52186), and kaempferol (Sigma-Aldrich, 60010) were the main active components of licorice analyzed in this study. A CCK-8 (Apexbio, USA) assay was used to evaluate the half-maximal inhibitory concentration (IC_{50}) and viability of the target cells. MKN-45 cells (1×10^5) were cocultured with 25 μM of the active components of licorice for 24 h. After the addition of the CCK-8 solution, the optical density at 405 nm was measured. The cells were inoculated in 96-well plates, and cell proliferation was observed using a high-content imaging analysis system after the addition of drugs. From 0 to 20 h, photos were taken every 3 h to collect the DPC signals produced by cells under drug treatment.

2.2. Calcein-AM/PI Double Staining. The calcein-AM/PI live/dead cell double staining kit was used to calculate the mortality rate of cancer cells after drug treatment. Adherent cells were trypsinized, and the supernatant was removed after centrifugation (1000 rpm for 3 min). The cells were thereafter washed 2-3 times with 1× assay buffer to remove esterase activity, and a cell suspension was prepared (1×10^5–1×10^6 cells/ml). Staining solution (100 μL) was added to 200 μl of cell suspension and incubated at 37°C for 15 min. FITC (green fluorescence, live cells) and PE signals (red fluorescence, dead cells) were detected using laser confocal fluorescence microscopy (OLYMPUS IX81).

$$\text{Mortality rate}\,(\%) = \left(\frac{\text{dead cell counts}}{\text{total cell counts}}\right) \times 100. \quad (1)$$

2.3. Cell Cycle Analysis. Cells at the logarithmic growth stage (2×10^5–1×10^6) were collected into 1.5 mL EP tubes and centrifuged, and the supernatant was discarded. The cells were washed once with PBS and centrifuged, and the supernatant was discarded. DNA staining solution (1 mL) and permeabilization solution (10 μL) were added and incubated at room temperature for 30 min in the dark. The proportion of G0/1, S, and G2M stage cells was recorded using flow cytometry (BD FACSCanto), and the proliferation index (PI) was calculated as follows:

$$\text{PI}\,(\%) = \frac{(S + G2M)}{(G0/1 + S + G2M)} \times 100. \quad (2)$$

A decrease in PI indicates the inhibition of proliferation, whereas an increase in PI indicates active proliferation.

2.4. AV/PI Staining and Hoechst Staining. Cell apoptosis was detected using the annexin V/propidium iodide (AV/PI) apoptosis kit (AP101, MULTI SCIENCES) and Hoechst 33342 (C0030, Solarbio). After treatment with the drugs for 24 h, 1×10^6–3×10^6 cells were collected, centrifuged twice with precooled PBS, and the supernatant was discarded. Then, 500 μl Apoptosis Positive Control Solution was added and incubated on ice for 30 min. The precooled PBS was centrifugally washed again, and the supernatant was discarded. An appropriate amount of precooled 1 × Binding Buffer and equivalent number of untreated live cells were added to the mixture. The precooled 1 × Binding Buffer was added to 1.5 ml tubes and equally divided into three tubes, one tube for the blank control and the other two tubes for single dye. Then, 5 μl Annexin V-FITC and 10 μl PI were added to the remaining dye tubes and incubated at room temperature for 5 min away from light. In flow cytometry (BD FACSCanto), the voltage of FSC, SSC, and fluorescence

channel was regulated using a blank tube, and the compensation of the fluorescence channel was regulated by a single dye tube under this voltage condition. The cells were stained with Hoechst 33342, and results were observed using a high-content analysis system (PerkinElmer Operetta CLS).

2.5. Mitochondrial Membrane Potential. The mitochondrial membrane potential of normal cells is high, forming a JC-1 polymer that emits strong red fluorescence (PE). In apoptotic cells, JC-1 is a monomer and emits green fluorescence (FITC) owing to a decrease in the mitochondrial membrane potential. Cells were collected in 6-well plates, 1 mL of JC-1 staining solution (tetrechloro-tetraethylbenzimidazol carbocyanine iodide) was added to each well, and the plates were incubated (37°C for 20 min). The cells were subsequently washed twice with JC-1 staining buffer (1X). Thereafter, 2 mL of the cell culture medium was added, and fluorescence signal values of the FITC and PE channels were observed using a high-content analysis system (PerkinElmer Operetta CLS). The mean fluorescence intensity ratio (MFIR) was used to evaluate changes in mitochondrial membrane potential. MFIR and mitochondrial membrane potential decreased, indicating an increase in apoptosis.

$$\text{MFIR} = \frac{\text{PE mean}}{\text{FITC mean}}. \tag{3}$$

2.6. Mitochondrial Morphology. After trypsinization, the cells were centrifuged, washed (PBS), fixed with 2.5% glutaraldehyde (2 h), and rinsed three times with phosphoric acid (0.1 M). The cells were then fixed (1% osmic acid for 2 h) and rinsed three times with phosphoric acid (0.1 M). Cells were sequentially treated with 50%, 70%, 90%, and 100% ethanol and 90% acetone. Finally, the cells were treated with 100% acetone (room temperature, 20 min), pure acetone and embedding solution (2 : 1, room temperature, 4 h), pure acetone and embedding solution (1 : 2, room temperature, overnight), or pure embedding solution (37°C, 3 h). The cells were incubated at 37°C (overnight), 45°C (12 h), and 60°C (48 h). Ultrathin (70 nm) microsheets were prepared and double stained with 3% uranium acetate and lead citrate. Finally, mitochondrial morphology was observed using a transmission electron microscope (HT7800, Hitachi).

MitoLiteM Red FX600 (AAT Bioquest) reagents are fluorogenic probes that label the mitochondria of live cells. Cells were grown in a 96-well plate (100 μL/well), and upon reaching the desired confluence, an equal volume of the dye-working solution was added. The cells were incubated in a 37°C, 5% CO_2 incubator for 2 h. The dye-loading solution was replaced. Mitochondrial morphology was observed using a high-content analysis system (PerkinElmer Operetta CLS).

2.7. The Network Pharmacology. The prediction of the pharmacokinetic properties and toxicity of compounds using computer technology can reduce the cost of drug evaluation and provide a reference for drug development. In this study, the ADMETlab 2.0 and ProTox-II databases were used to evaluate the ADMET properties, LD_{50}, and potential toxicity of the active components of licorice.

The potential targets of licorice were screened using the Traditional Chinese Medicine Systems Pharmacology (TCMSP) Database. Target protein names were converted into gene IDs using the Universal Protein database. We obtained gastric cancer-related targets from the following databases using the keywords "gastric cancer": Online Mendelian Inheritance in Man (OMIM), DrugBank, Therapeutic Target Database (TTD), GeneCards, PharmGKB, and DisGeNET. Literature relevant to gastric cancer was searched using PubMed, China National Knowledge Infrastructure (CNKI), and Wanfang data. After mapping "potential targets of licorice" and "gastric cancer-related targets" to each other, we obtained the "common targets" and generated a Venn diagram using an online tool.

The protein-protein interaction (PPI) network of common targets was obtained using the Search Tool for the Retrieval of Interacting Genes (STRING). The parameters were as follows: organism was "*Homo sapiens*," minimum required interaction score was medium (confidence >0.4), and the others were default. The topological parameters of the PPI network included degree, BC, and CC; "degree" represents the degree of a node, and BC and CC represent the shortest path crossing a single node and the ease of communication between nodes, respectively. Visual analysis and topological parameters of the PPI network were obtained using Cytoscape 3.7.2, and clustering analysis was performed using the molecular complex detection algorithm.

Kyoto Encyclopedia of Genes and Genomes (KEGG) enrichment analyses were performed using the Metascape database, and chord diagrams were drawn online (https://www.bioinformatics.com.cn).

2.8. Molecular Docking and Dynamics Simulation. The receptor proteins were downloaded from the RCSD database as the crystal structures of the molecular docking proteins. The PrepWiz module in Schrödinger 2020-4 software was used to predispose the protein crystal structure by adding hydrogen, removing water molecules, and completing the side chains. Molecular docking was performed using Glide's standard precision method. In this study, a docking score of ≤ -5 for a compound indicated its potential activity. Simultaneously, the molecular mechanics with generalized Born and surface area solvation (MM/GBSA) method was used to estimate binding energy based on the docking score of the original ligand in the protein crystal structure.

In the Gaussian 16 program, the HF/6-31 (d, p) group was used to optimize the structure of astragalus small-molecule compounds and calculate RESP charges. The Amber 20 software package was used for the molecular dynamics simulation, and the Langevin thermostat was used to gradually heat the complex system from 0 to 310 K and simulate 400 ps. The system temperature was maintained at 310 K, and an equilibrium simulation was performed at 200 ps. Finally, a 50 ns molecular dynamics simulation of the

EGFR protein complex system was performed in the N_PT ensemble. The temperature and pressure were set to 310 K and 1 bar, respectively, and the periodic boundary conditions were set. Electrostatic calculations were performed using PME with a cutoff value of 10 A.

To explore the binding details between proteins and ligands and screen residues that contribute significantly to binding, the MM/GBSA method was adopted in the MMPBSA.py program of the Amber 20 software package to capture the last 10 ns molecular dynamics simulation locus of the complex system of each active component of licorice with the core target; 100 frames were extracted at equal time intervals for residue energy decomposition calculations.

2.9. Western Blot Analysis. Cell lysate proteins were separated using 10% sodium dodecyl sulfate-polyacrylamide gel electrophoresis and transferred onto a polyvinylidene difluoride membrane. The membranes were incubated with MEK1 (ab32091, Abcam, USA), phospho-MEK1 (ab96379, Abcam, USA), ERK1 (ab119357, Abcam, USA), phospho-ERK1 (ab194776, 1 : 500, Abcam, USA), and GAPDH (5174, CST, Danvers, MA, USA; 4°C overnight). Secondary antibodies (anti-rabbit IgG, RS0002, and Immunow) were added and incubated (room temperature for 2 h). After washing, the ECL working liquid is dripped onto the film for development and fixing. After membrane exposure, we analyzed the gray value of the protein bands (ImageJ) and calculated their relative expression (relative expression = target protein expression/GAPDH expression).

2.10. Immunofluorescence. After the drug-treated cells were immobilized with paraformaldehyde, paraformaldehyde-fixed cells were incubated with antibodies against ERK1/2 (Plano, TX, USA), PTGS2 (Hangzhou, China), Cyt-C (HUABIO, ET1610-60), and BCL-2 (HUABIO, ET1702-53; 4°C, overnight). Then, secondary antibodies were added and incubated (room temperature for 2 h). Finally, the protein expression levels in target cells were observed using a high-content analysis system (PerkinElmer Operetta CLS) and laser confocal fluorescence microscopy (OLYMPUS IX81).

2.11. Immunohistochemistry. The slides were incubated with Ki67 (Servicebio, GB111499, diluted at 1 : 500), BCL-2 (Servicebio, GB114830), caspase 3 (Servicebio, GB11532, diluted at 1 : 500), and BAX (Servicebio, GB114122, diluted at 1 : 500) antibodies overnight at 4°C. After rinsing with PBS, secondary antibodies (HRP goat anti-rabbit IgG, Servicebio, GB23303, diluted at 1 : 200) were added and incubated (37°C for 10 min). After DAB color development, a panoramic histiocytic quantification system (TissueFAXS Plus, TissueGnostics Asia Pacific Limited) was used. Ki67+ cell counts and integrated option density (IOD) of apoptotic proteins (caspase 3, BCL-2, and BAX) were computed using ImageJ software.

$$\begin{aligned}\text{Ki67 percentage}\,(\%) &= \left(\frac{\text{Ki67 + cell count}}{\text{total cell count}}\right) \times 100,\\ \text{average optical density}\,(\text{AOD}) &= \frac{\text{IOD}}{\text{Area}},\end{aligned} \tag{4}$$

where AOD was proportional to the expression of target protein.

2.12. Terminal Deoxynucleotidyl Transferase-Mediated dUTP-Biotin Nick End Labeling (TUNEL) Assay. Nuclei stained with DAPI were blue under ultraviolet light excitation; the TUNEL kit (Servicebio, G1501) was labeled with FITC fluorescein, and the positive apoptotic cells were labeled with green light (FITC). Images were obtained using a panoramic histiocytic quantification system (TissueFAXS Plus, TissueGnostics Asia Pacific Limited).

2.13. Humanized Mouse Tumor Models. A mouse model of gastric cancer was generated using the method outlined by Zhang [12]. Mice were intraperitoneally administered antitumor drugs (20 mg/kg daily for 15 d). Untreated mice were used as the model (control) group. After the experiment, the tumor volume and weight were recorded, and the tumor inhibition rate was calculated as follows:

$$\begin{aligned}\text{tumor volume} &= \frac{(\text{long diameter}) \times (\text{shorter diameter})^2}{2},\\ \text{tumor inhibition rate}\,(\%) &= \frac{(\text{average mass of model group} - \text{average mass of intervention group})}{\text{average mass of model group} \times 100}.\end{aligned} \tag{5}$$

Hematoxylin-eosin (H&E) staining, immunofluorescence, immunohistochemistry, and TUNEL assay were performed on tumor tissues.

2.14. Statistical Analysis. The mean ± standard deviation (SD) of three independent experiments was recorded. Differences between two groups were evaluated using two-way ANOVA and Student's *t*-test in GraphPad Prism 5. $p < 0.05$ indicated differences between two groups; $p < 0.01$ indicated a significant difference; $p < 0.001$ indicated a highly significant difference; and $p > 0.05$ indicated no significant difference. Finally, histograms and line charts were created using the GraphPad Prism software.

3. Results

3.1. The IC_{50} of Licorice-Active Component. In previous experiments, we found that five common licorice-active components (quercetin, kaempferol, isorhamnetin, naringenin, and licochalcone A) may inhibit gastric cancer. Most drugs are unstable or toxic, and undesirable pharmacokinetic properties and toxicity are major causes of drug candidate development failure. Therefore, we evaluated the absorption, distribution, metabolism, excretion, and toxicity (ADMET) properties and toxicity using the ADMETlab and ProTox-II databases. In Figures 1(a)–1(c), according to the toxicity class, these active compounds of licorice were considered safe and could be further developed as TCM monomers. The half-maximal inhibitory concentration (IC_{50}) and cytotoxicity of the drugs were detected using the CCK-8 assay; the lower the IC_{50} value, the stronger the inhibitory effect. As shown in Figure 1(d), quercetin exhibited the lowest IC_{50} values (28.54 μmol/L), and its cytotoxic effect on MKN-45 cells was significantly stronger than that of the others ($p < 0.001$). Therefore, quercetin was selected for follow-up experiments.

3.2. Quercetin Treatment Inhibits Cell Proliferation of MKN-45. After H&E staining, the control group was characterized by uniform cell morphology, a complete nucleus and cytoplasm, and a good cellular state. After adding quercetin, cell morphology changed to include hyperchromatic and pyknotic cell nuclei and blurred boundaries between the nucleus and cell membrane (Figure 2(a)). A similar trend was observed for the lapatinib group.

We found significant differences between the drug group (quercetin and lapatinib groups) and the control group from day 14 onwards; MKN-45 cells in the control group grew normally and proliferated rapidly, whereas those in the quercetin or lapatinib group proliferated slowly (Figure 2(b)). After quercetin and lapatinib treatment, the mortality rate of MKN-45 cells reached 28.1% and 36.9%, respectively, which was significantly higher than that of the control group (4.3%; Figure 2(c)).

In the control group (Figure 2(d)), the proportion of "S + G2M stage" was 51.3%; after drug treatment, it significantly decreased ($p < 0.001$; quercetin group: 32.31% and lapatinib group: 33.47%), indicating that cell proliferation was inhibited by external factors. These results indicated that quercetin could effectively inhibit the proliferation of MKN-45 cells and accelerate their death.

3.3. Quercetin Treatment Promotes Cell Apoptosis of MKN-45. Cell death occurs via two main pathways: apoptosis and necrosis. Promoting the apoptosis or necrosis of cancer cells is an important means of cancer therapy and one of the main ideas for developing antitumor drugs.

A scatter plot (Figure 3(a)) was used to distinguish among living, apoptotic, and necrotic cells. We found that cell apoptosis in the control group was not obvious and that in the quercetin group, 24.9% of cells were necrotic and 10.2% of cells were in late apoptosis, whereas in the lapatinib group, necrotic and apoptotic cells accounted for 21.1% and 12%, respectively. As shown in Figure 3(b) and Video 1–3, after Hoechst 33342 staining, the nuclei of the living cells showed uniform and diffuse fluorescence in the control group. In contrast, in the quercetin and lapatinib groups, the nucleus or cytoplasm was deeply stained (dense clumps of fluorescent particles) and the apoptosis rate of MKN-45 cells was significantly increased ($p < 0.001$). Compared with the control group, the expression level of Cyt-C in the quercetin and lapatinib groups increased and that of BCL-2 (anti-apoptotic protein) decreased ($p < 0.001$; Figure 3(c)). Hence, cell apoptosis was promoted.

Mitochondria are the centers of cellular energy metabolism. Normal mitochondria are long; when cells undergo apoptosis through the mitochondria-related pathway, they undergo a series of changes, such as mitochondrial swelling and reduction or breakage of ridges, vacuoles, and decreased mitochondrial membrane potential. As shown in Figure 3(d), compared to the control group, the mitochondrial membrane potential in the quercetin and lapatinib groups was significantly decreased ($p < 0.001$). Moreover, after quercetin treatment, there were some apoptotic cells (a complete nuclear membrane, visible cell membrane, and hyperchromatic and pyknotic cell nuclei), and their mitochondrial morphology varied greatly (e.g., mitochondrial swelling, ridge fracture, and vacuoles; Figures 3(e) and 3(f)). These results indicated that quercetin promotes mitochondria-mediated endogenous apoptosis.

3.4. The Network Pharmacology of Quercetin against Gastric Cancer. In an in vitro experiment, quercetin promoted apoptosis and mitochondrial damage in gastric cancer cells, but the molecular mechanism remains unclear. Network pharmacology was used to predict the key targets and signaling pathways of quercetin against gastric cancer. Initially, 142 potential targets of quercetin were identified using the TCMSP platform. We then collected 499, 92, 36, 314, 134, and 1520 gastric cancer-related targets from the OMIM, DrugBank, TTD, PharmGKB, DisGeNET, and GeneCards databases, respectively. After merging and removing duplicates, we obtained 2226 gastric cancer-related targets (Figure 4(a)). These targets were compared with the potential targets, and a Venn diagram was obtained for 106 common targets (Figure 4(b)).

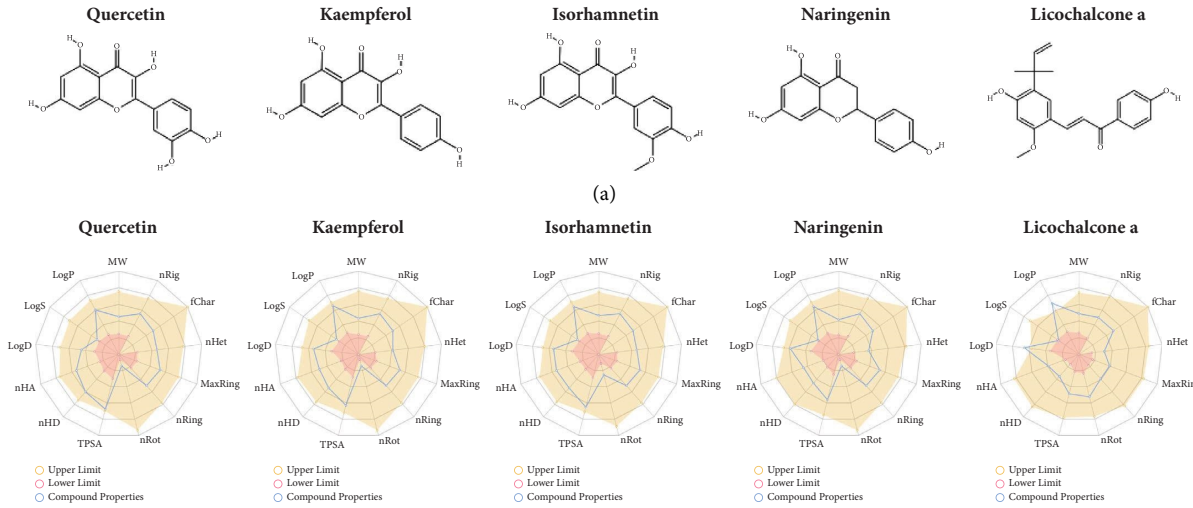

(a)

(b)

The toxicity prediction of five main active compounds.

Full mame	OB (%)	DL	Hepatotoxicity		Carcinogenicity		Immunotoxicity		Mutagenicity		Cytotoxicity		LD50 (mg/kg)	Toxicity Class
			Toxicity	Probability	Toxicity	Probability	Toxicity	Probability	Toxicity	Probability	Toxicity	Probability		
Quercetin	46.43	0.28	Inactive	0.69	Active	0.68	Inactive	0.87	Active	0.51	Inactive	0.99	159	III
Kaempferol	41.88	0.24	Inactive	0.68	Inactive	0.72	Inactive	0.96	Inactive	0.52	Inactive	0.98	3919	V
Isorhamnetin	49.6	0.32	Inactive	0.72	Inactive	0.68	Active	0.58	Inactive	0.94	Inactive	0.95	5000	V
Naringenin	59.29	0.21	Inactive	0.67	Inactive	0.62	Inactive	0.88	Inactive	0.83	Active	0.59	2000	IV
Licochalcone a	40.79	0.29	Inactive	0.62	Inactive	0.6	Active	0.76	Inactive	0.79	Inactive	0.77	1000	IV

(c)

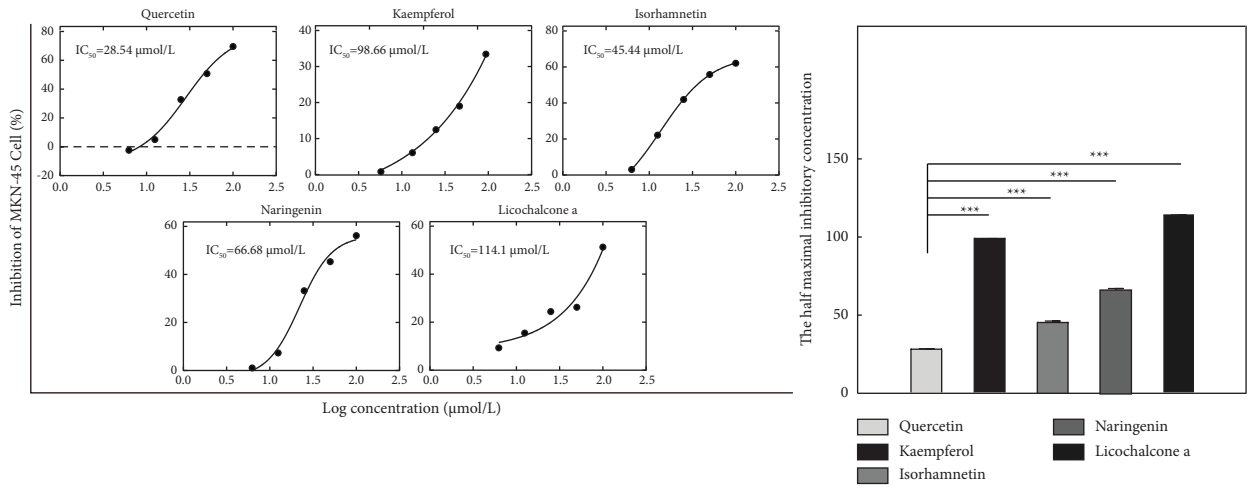

(d)

Figure 1: Active components in licorice. (a) The 2D structure. (b) The ADMET property. (c) The toxicity prediction. Oral bioavailability (OB) exceeding 30% reduces the amount of an administered drug necessary to achieve a desired pharmacological effect and, therefore, could reduce the risk of side-effects and toxicity. Drug-likeness (DL) exceeding 0.18 was considered as having good drug-likeness. LD50: lethal dose 50%. Toxicity class I: fatal if swallowed (LD50 ≤ 5 mg/kg); toxicity class II: fatal if swallowed (5 < LD50 ≤ 50 mg/kg); toxicity class III: toxic if swallowed (50 mg/kg < LD50 ≤ 300 mg/kg); toxicity class IV: harmful if swallowed (300 mg/kg < LD50 ≤ 2000 mg/kg); toxicity class V: may be harmful if swallowed (2000 mg/kg < LD50 ≤ 5000 mg/kg); toxicity class VI: nontoxic (LD50 > 5000 mg/kg). (d) The IC50 of active components in licorice. IC50: half-maximal inhibitory concentration. $^{*}p < 0.05$ indicates differences between two groups; $^{**}p < 0.01$ was considered to be a significant difference; $^{***}p < 0.001$ was considered to be a highly significant difference.

The PPI network shows the interaction of 106 common targets, which contains 106 nodes and 2215 edges (Figure 4(c)). We screened out 10 key targets based on topological parameters (degree, betweenness centrality, and closeness centrality), i.e., tumor protein p53 (TP53), AKT serine/threonine kinase 1 (AKT1), tumor necrosis factor

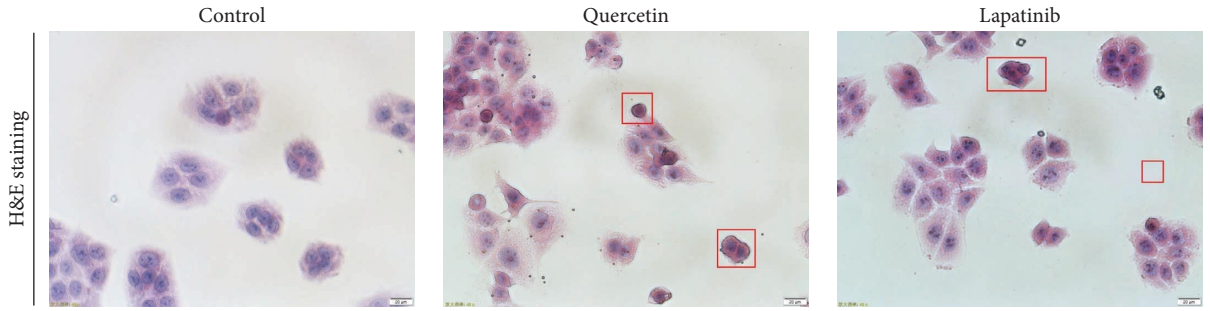

(a)

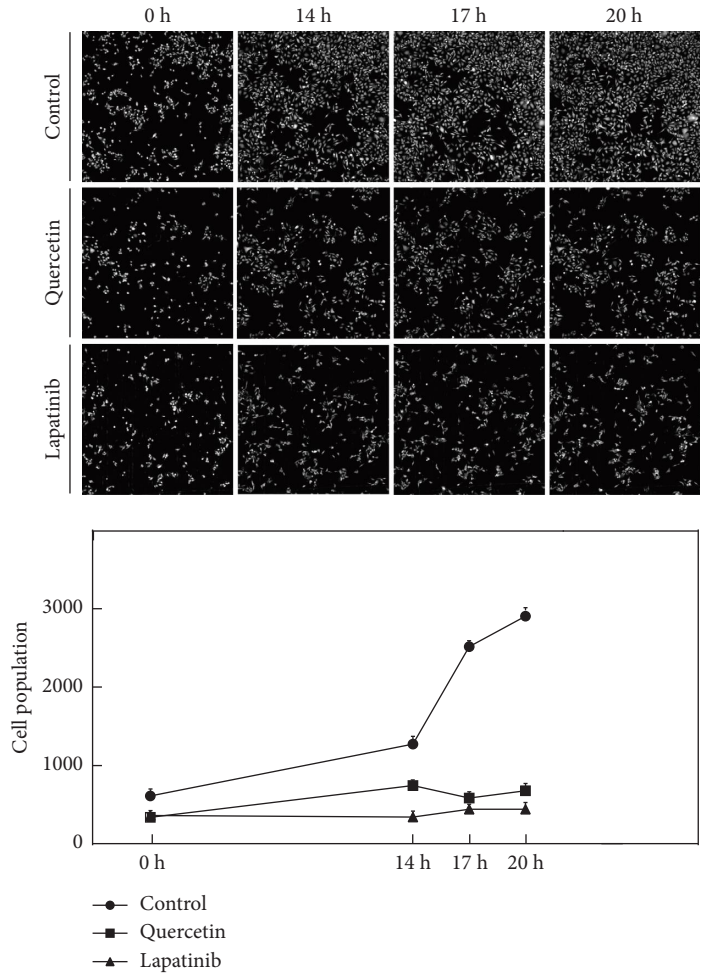

(b)

Figure 2: Continued.

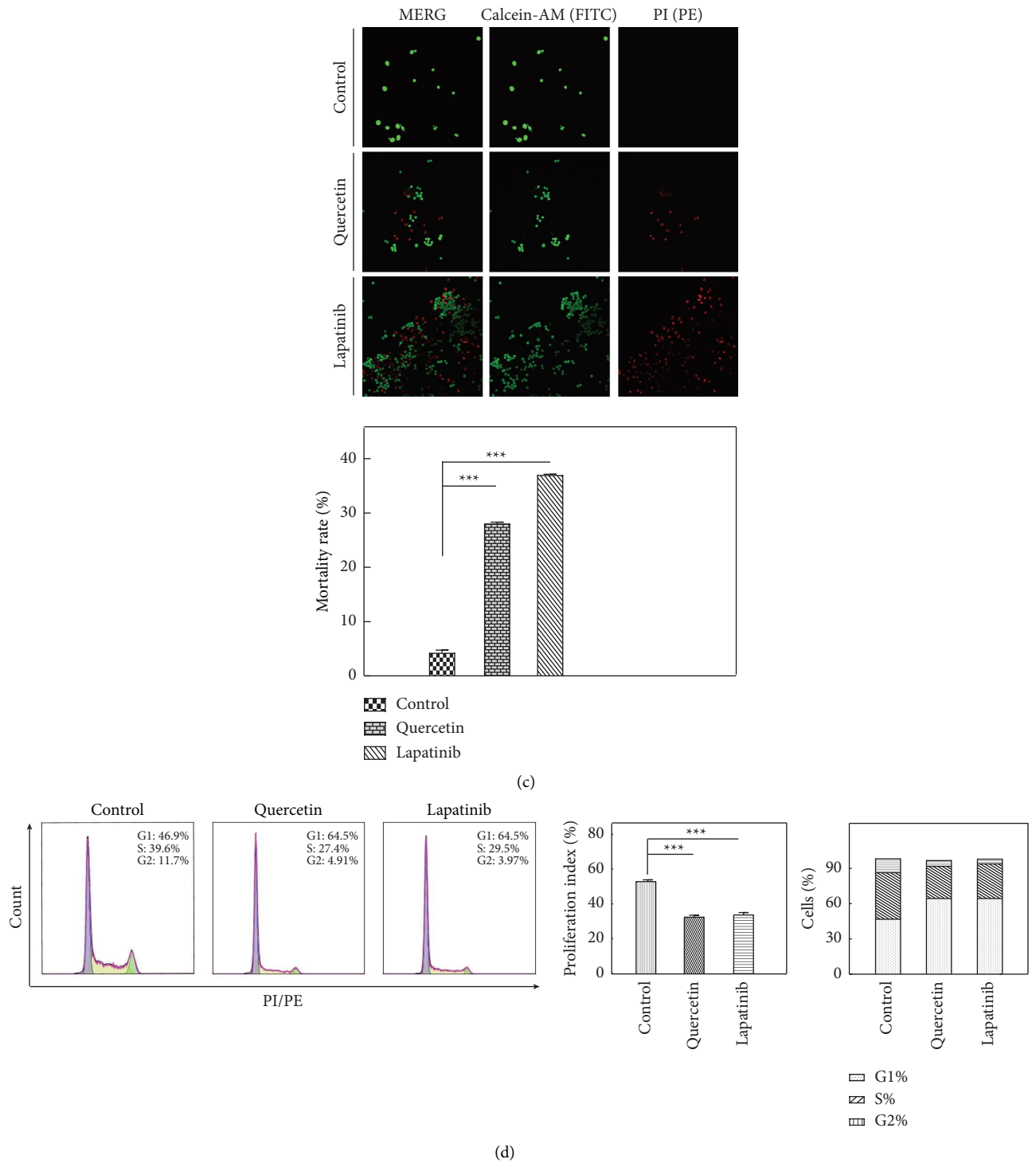

Figure 2: Quercetin treatment inhibits cell proliferation of MKN-45. (a) H&E staining. (b) Cell proliferation. (c) The mortality rate of MKN-45. (d) The cell cycle. $^{*}p < 0.05$ indicates differences between two groups; $^{**}p < 0.01$ was considered to be a significant difference; $^{***}p < 0.001$ was considered to be a highly significant difference.

(TNF), caspase 3 (CASP3), interleukin 6 (IL6), estrogen receptor 1 (ESR1), Jun proto-oncogene AP-1 transcription factor subunit (JUN), epidermal growth factor receptor (EGFR), hypoxia inducible factor subunit alpha (HIF1A), and B-cell lymphoma-2 (BCL-2). The TTD database was used to verify information about these key targets, including clinical trials and listed drugs, with a focus on selecting targets of marketed antitumor drugs. Three targets (BCL-2, EGFR, and ESR1) were associated with cancer-related drugs and were mainly targeted in the treatment of chronic

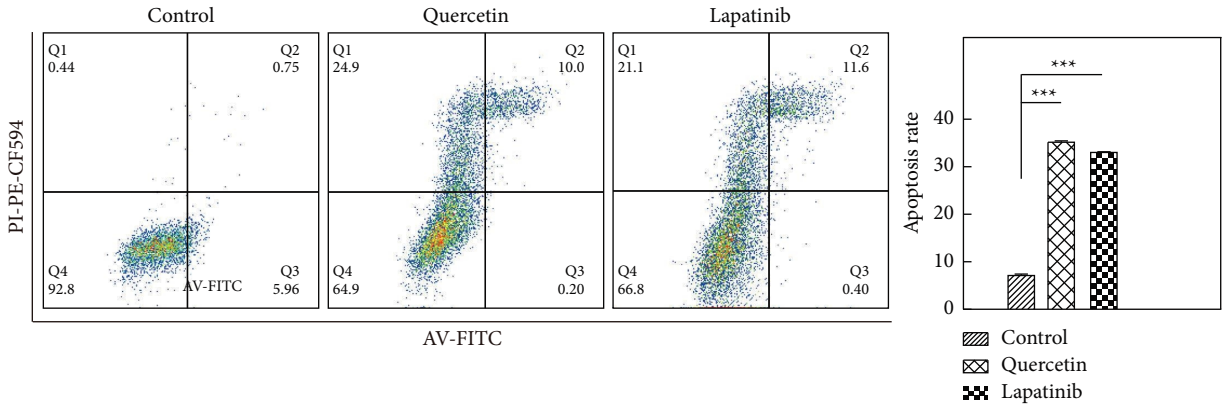

(a)

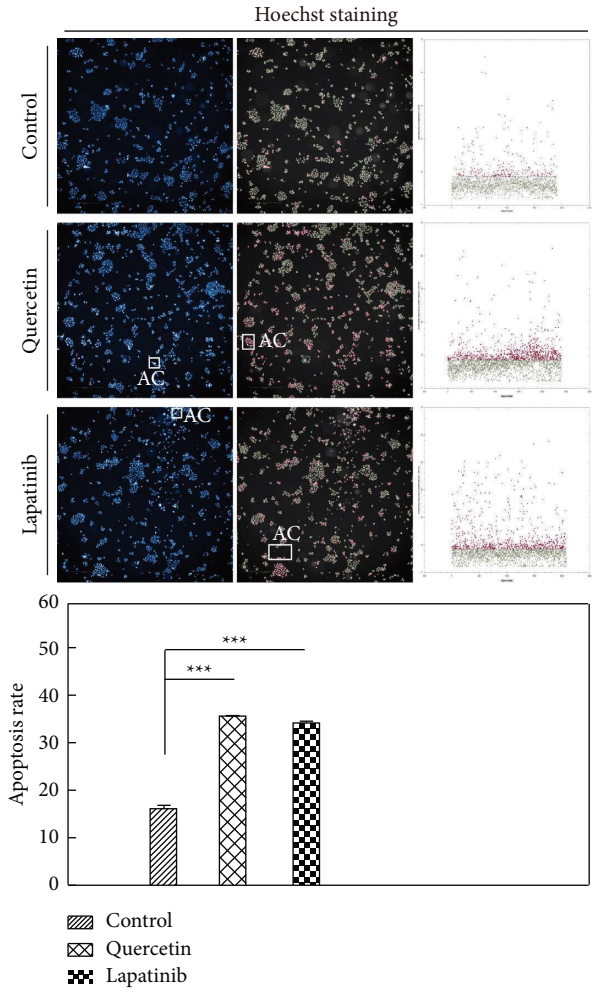

(b)

Figure 3: Continued.

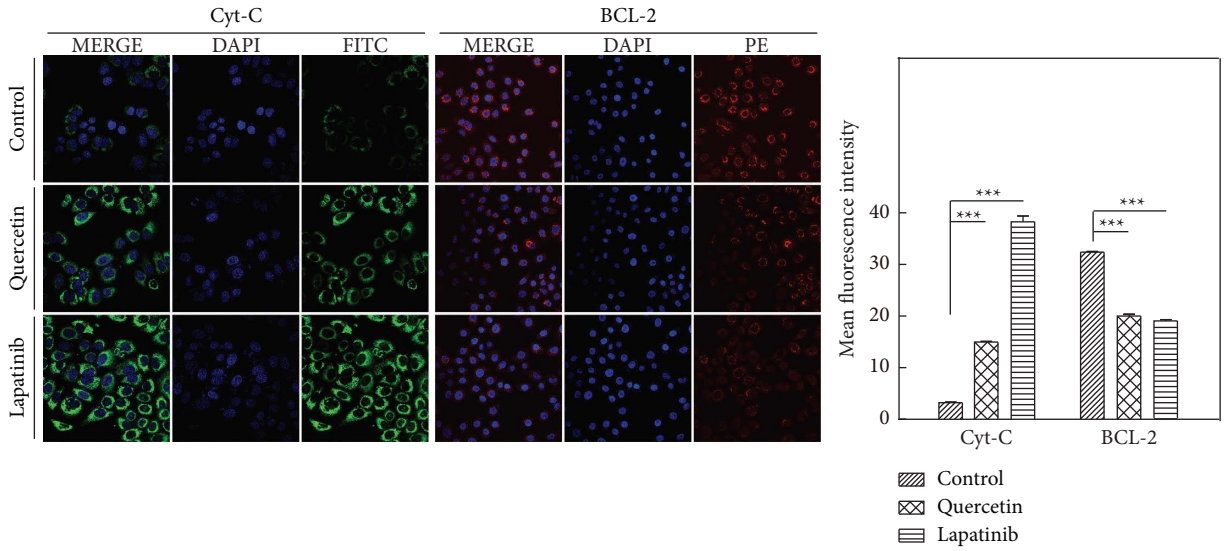

(c)

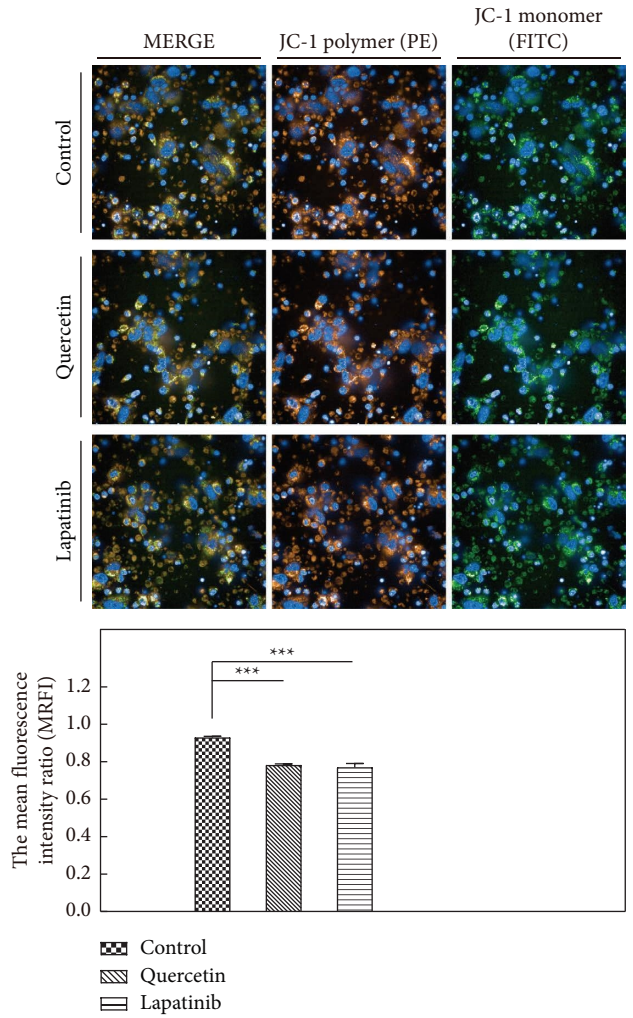

(d)

Figure 3: Continued.

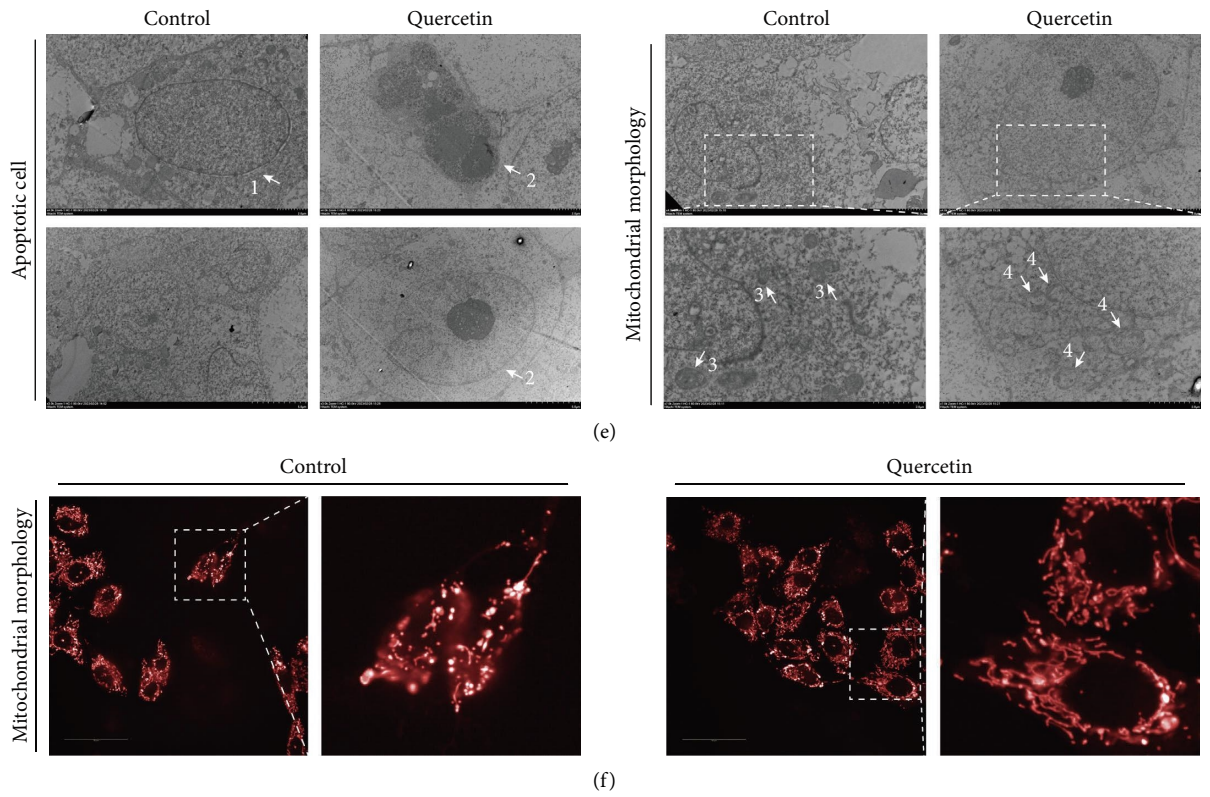

Figure 3: Quercetin treatment promotes cell apoptosis of MKN-45. (a) Flow cytometric analysis of cell apoptosis (AV/PI staining). (b) High-content analysis of cell apoptosis (Hoechst 33342 staining). AC: apoptotic cell. (c) The expression of apoptosis-related factors. (d) The mitochondrial membrane potential. (e) The mitochondrial damage (transmission electron microscopy). (f) The mitochondrial damage (high-content analysis system). 1: normal cells; 2: apoptotic cells (complete nuclear membrane, visible cell membrane, and hyperchromatic and pyknotic cell nucleus); 3: normal mitochondria; 4: mitochondrial swelling, ridge fracture. $^{*}p < 0.05$ indicates differences between two groups; $^{**}p < 0.01$ was considered to be a significant difference; $^{***}p < 0.001$ was considered to be a highly significant difference.

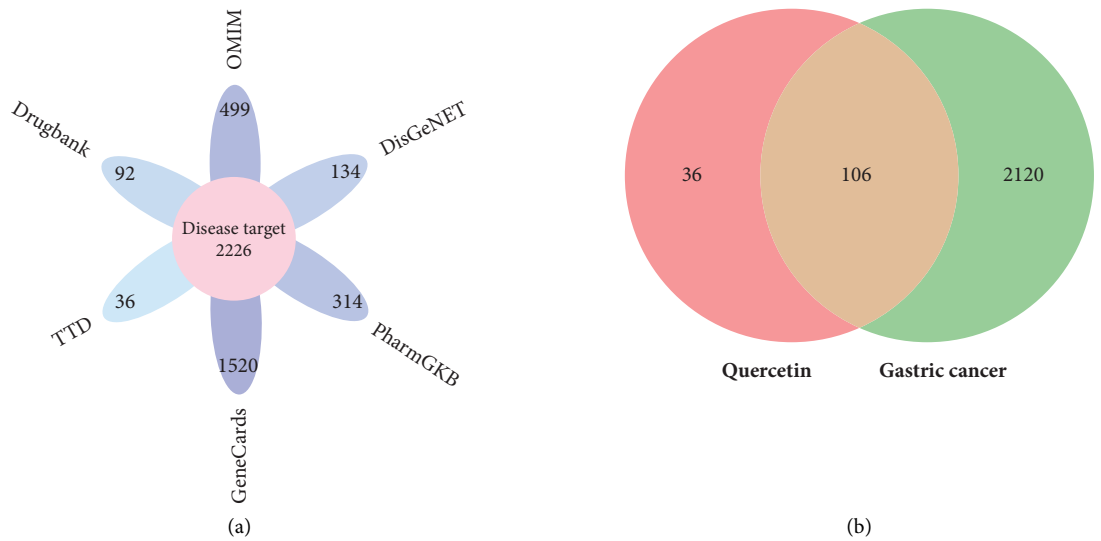

Figure 4: Continued.

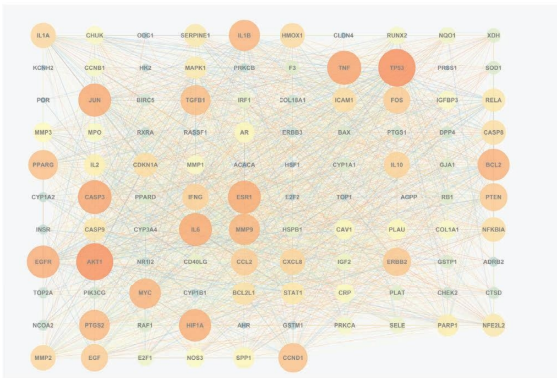

(c)

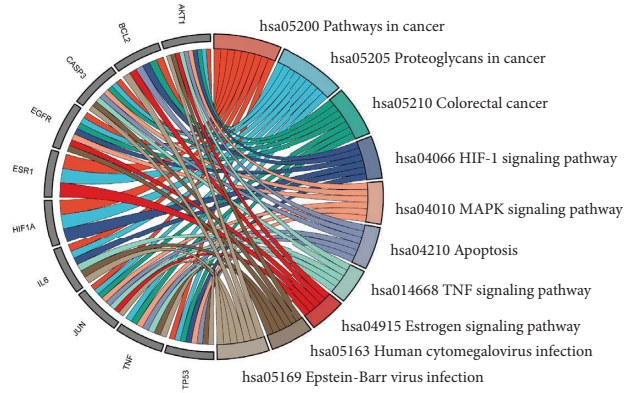

(d)

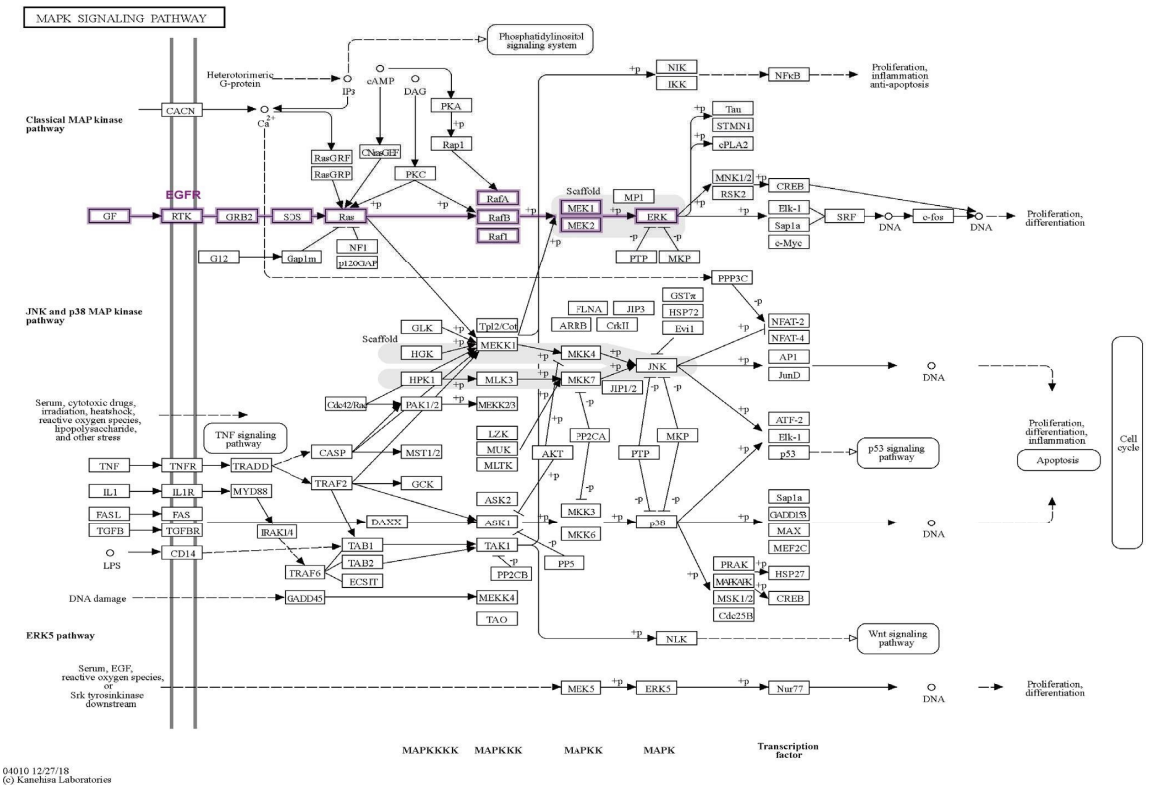

(e)

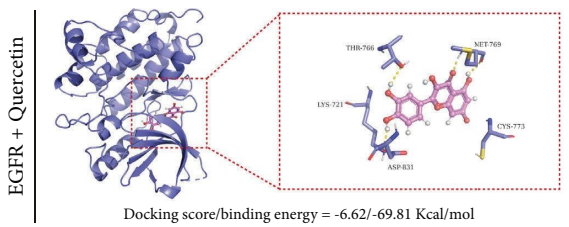

(f)

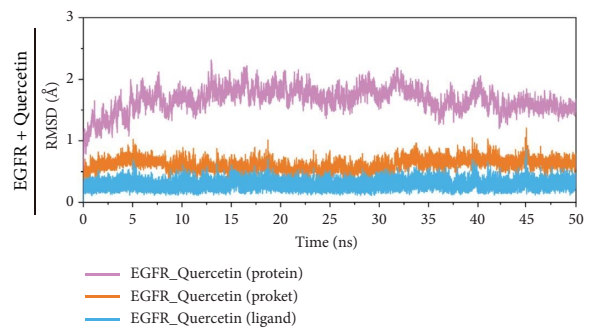

(g)

Figure 4: Continued.

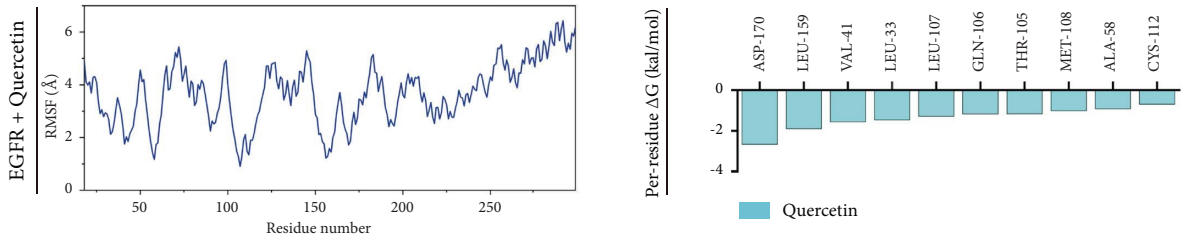

Figure 4: Network pharmacology and the molecular docking. (a) The gastric cancer-related targets. (b) Venn diagram of the targets in licorice and gastric cancer. (c) The PPI network. (d) KEGG enrichment analysis. (e) The map of the ERK signal pathway (this image was from the KEGG database and the purple box is "EGFR-ERK signaling pathway). (f) Molecular docking (the molecular docking results are from Schrodinger 2020-4 software and a docking score of ≤ −5 for a compound indicated its potential activity). (g) The RMSD fluctuations over time of the "EGFR-quercetin" complex system. (h) The RMSF of each residue of the "EGFR-quercetin" complex system during the molecular dynamics (last 10 ns). (i) The binding energy of the top ten residues that contribute most to ligand binding in the "EGFR-quercetin" complex system. RMSD, root mean square deviation and RMSF, root mean square fluctuation.

myelogenous leukemia, acute lymphoblastic leukemia, breast cancer, and nonsmall cell lung cancer. Four target drugs have been used to treat cancer in clinical trials (CASP3, HIF1A, IL6, and TP53).

However, none of these targets has been described as being involved in gastric cancer, and no clinical trials or retrospective studies of gastric cancer have been found. KEGG enrichment analysis was performed for these targets. The pathways associated with cancer are shown in Figure 4(d). Previous studies have shown that the EGFR and MAPK pathways are involved in the development and occurrence of gastric cancer, and EGFR is a key molecule upstream of the ERK/MAPK single pathway. Combined with the network pharmacological results, we speculated that the mechanism of quercetin against gastric cancer was related to the EGFR-ERK signaling pathway (Figure 4(e)).

3.5. Molecular Docking and Dynamics. Molecular docking is an important technique in the field of computer-aided drug design, which makes research more efficient, economical, and predictable. Molecular docking analyses were performed between quercetin and EGFR (PDB ID: 4HJO, EM resolution: 2.75 Å, ligand: AQ4, and method: RAY) to predict their binding affinity. Docking scores and binding energies are often used to explain the binding strength of components and targets, which are important for evaluating molecular activity, with a docking score ≤−5 indicating that a compound has potential activity. The smaller the binding energy, the greater the binding potential. We found that EGFR had good binding ability to quercetin, with a low docking score and binding energy (Figure 4(f)). Quercetin was mainly bound to MET-769, THR-766, LYS-721, CYS-773, and ASP-831 residues of EGFR.

Molecular dynamics simulation was conducted for the "EGFR-quercetin" complex systems (Figure 4(g)). The root mean square deviation (RMSD) was used to evaluate the structural stability of the systems. We calculated the RMSD of the protein α-carbon atoms in each conformation of the trajectory relative to the initial structure, which remained in equilibrium during the entire simulation process. By evaluating the RMSD of α-carbon atoms in ligand 5 Å, we found that the binding sites of the systems were also relatively stable during the 50 ns simulation process. In addition, the RMSD values of the nonhydrogen ligands were calculated. Quercetin showed small RMSD fluctuations with EGFR during molecular dynamics simulation, indicating that quercetin could stably bind to EGFR. To evaluate the flexibility of the associated complex structures, the root mean square fluctuation (RMSF) of the last 10 ns of amino acid α-carbon atoms during the molecular dynamics simulation was calculated. As shown in Figure 4(h), RMSD and RMSF analyses revealed that quercetin was highly stable in the binding site region of EGFR. To identify the key residues closely related to biological activity, free-energy decomposition was used to calculate the specific binding free energy between the inhibitors and each residue in these systems, and the total binding free energy was calculated for each residue. Figure 4(i) shows the top ten residues that contributed most to ligand binding. We found that the most important residues in the "EGFR-quercetin" complex were ASP-170, LEU-159, VAL-41, LEU-33, and LEU-107.

3.6. Quercetin Treatment Affects ERK/MAPK Signaling Pathway Activity. Extracellular signal-regulated kinase 1/2 (ERK1/2) and mitogen extracellular kinase 1/2 (MEK1/2) are core proteins in the ERK/MAPK signaling pathway, and their activation is related to cell proliferation, apoptosis, cell cycle, and other processes. High levels of phospho-ERK1/2 (p-ERK1/2) or phospho-MEK1/2 (p-MEK1/2) indicate activation of the ERK/MAPK signaling pathway. Prostaglandin-endoperoxide synthase 2 (PTGS2) is located downstream of the ERK/MAPK signaling pathway, and its expression reflects whether the ERK/MAPK signaling pathway is activated or inhibited.

As shown in Figures 5(a) and 5(b), compared to the control group, p-MEK1, p-ERK1, and PTGS2 levels were significantly decreased in the quercetin and lapatinib groups ($p < 0.001$). These results indicated that the ERK signaling pathway was inhibited and PTGS2 expression was down-regulated in MKN-45 cells after quercetin and lapatinib treatment.

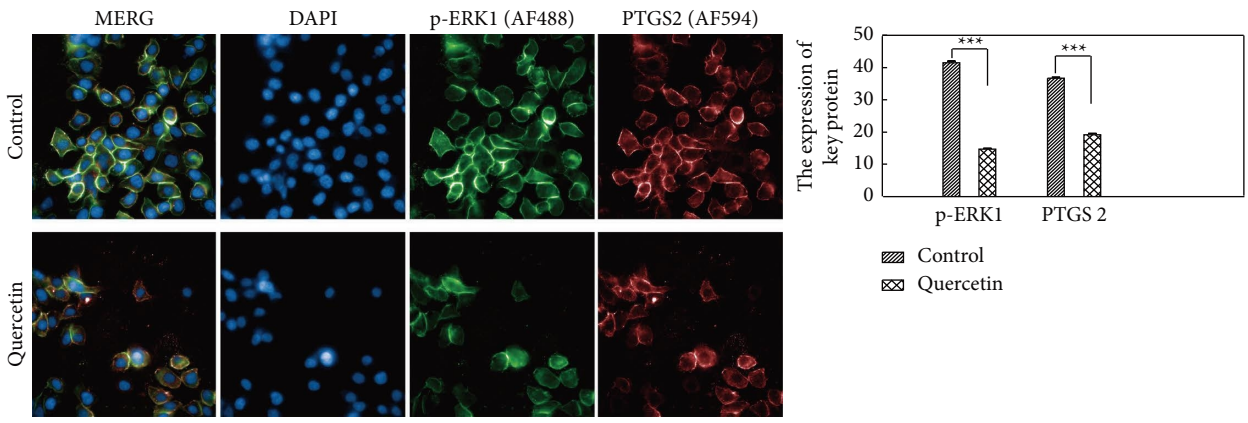

(a)

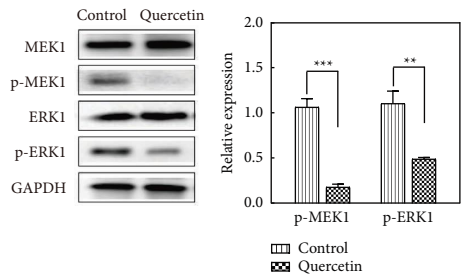

(b)

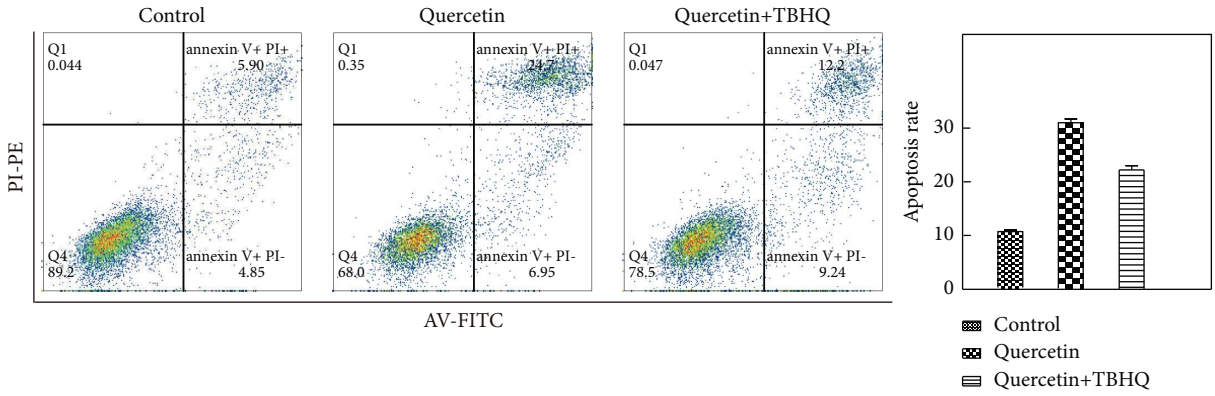

(c)

Figure 5: Continued.

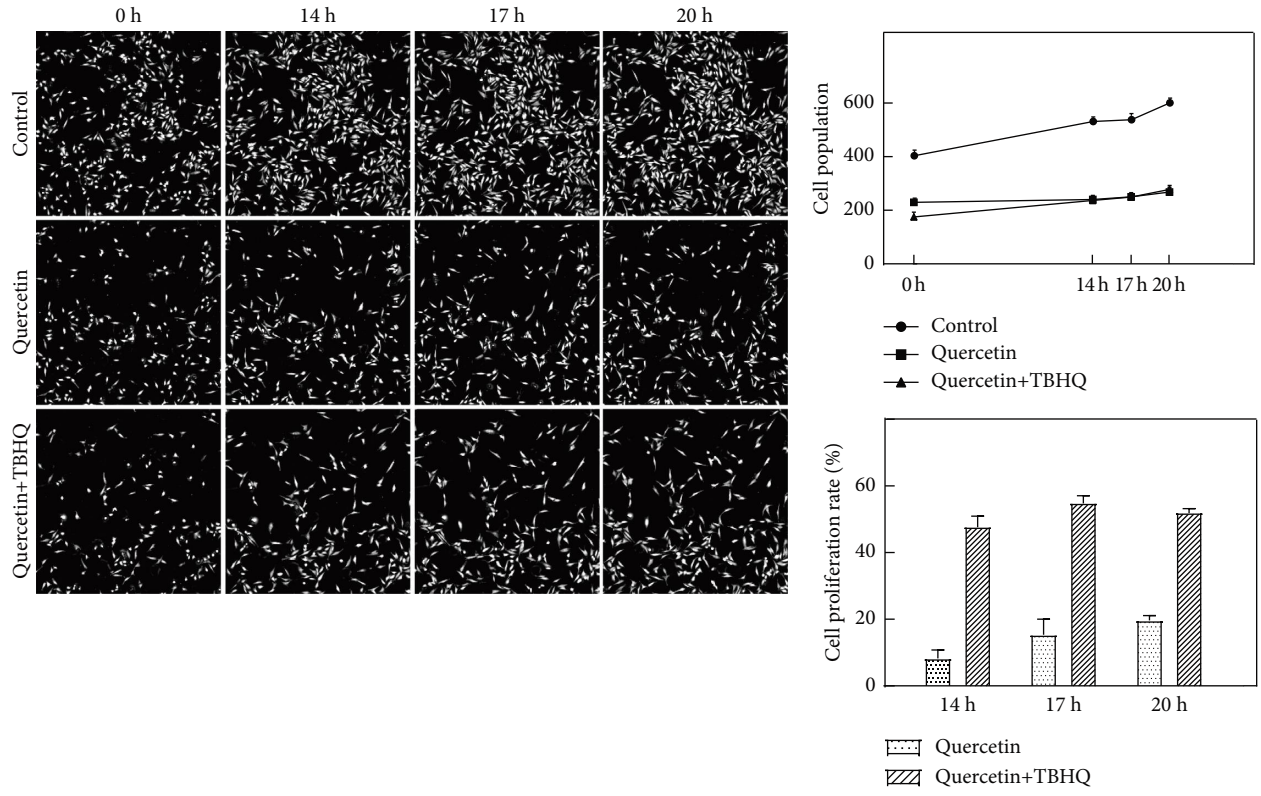

(d)

Figure 5: The expression of p-ERK1 and PTGS2 (high-content analysis system). (a) The expression of p-ERK1 and PTGS2 (high-content analysis system). (b) The expression of p-MEK1 and p-ERK1 (western blot). (c) Cell apoptosis. (d) Cell proliferation. $^{*}p < 0.05$ indicates there was a differences between two groups; $^{**}p < 0.01$ was considered to be a significant difference; $^{***}p < 0.001$ was considered to be a highly significant difference.

To verify the abovementioned results, we treated MKN-45 cells with quercetin alone or in combination with TBHQ (an ERK agonist) and detected cell apoptosis and cell proliferation. As shown in Figures 5(c) and 5(d), compared with the control group, apoptosis in the quercetin group was significantly increased and cell proliferation slowed down. However, this phenomenon was suppressed when quercetin was combined with TBHQ. Thus, quercetin plays an anti-gastric cancer role by blocking the EGFR-ERK signaling pathway.

3.7. Quercetin Treatment Inhibits Gastric Cancer Growth in Mouse Tumor Models. In the in vitro experiment, compared with the model group, the tumor volume of mice in the quercetin group ($p < 0.01$) and the lapatinib group ($p < 0.001$) was significantly reduced, and the tumor inhibition rates were 16.2% and 22.5%, respectively (Figures 6(a) and 6(b)).

The results of H&E staining of the tumor tissues are shown in Figure 6(c). In the model group, tumor cells had a high density, compact arrangement, more heteronuclear nuclei, and fewer infiltrating lymphocytes in the surrounding connective tissue. After dosing (quercetin and lapatinib groups), necrotic foci appeared in the tumor tissue.

In the quercetin group, mitochondrial damage, such as mitochondrial swelling and mitochondrial ridge fracture, was observed in both tumor and paracancerous tissues. In contrast, the model group had normal mitochondria (Figure 6(d)). In the TUNEL assay, the apoptotic signal (FITC) was stronger in the drug groups (quercetin and lapatinib) than in the model group ($p < 0.05$; Figure 6(e)).

Ki67 reflects the proliferative activity of tumor cells. Caspase 3, BAX, and BCL-2 are key apoptotic factors in the mitochondrial endogenous apoptotic pathway. Compared with the model group, after quercetin or lapatinib treatment, the Ki67 percentage was significantly decreased in mouse tumor tissue ($p < 0.001$), and the proliferation of tumor cells was slow. Meanwhile, caspase 3 and BAX increased ($p < 0.05$) and BCL-2 decreased ($p < 0.05$; Figure 6(f)). These results indicate that quercetin has a good antitumor effect in vivo.

4. Discussion

Licorice, one of the most common TCM, is used in numerous clinical formulations, which has earned it the reputation of "nine licorice in ten prescriptions." In this study, we found that quercetin was the main active component of licorice against gastric cancer. In previous studies, quercetin

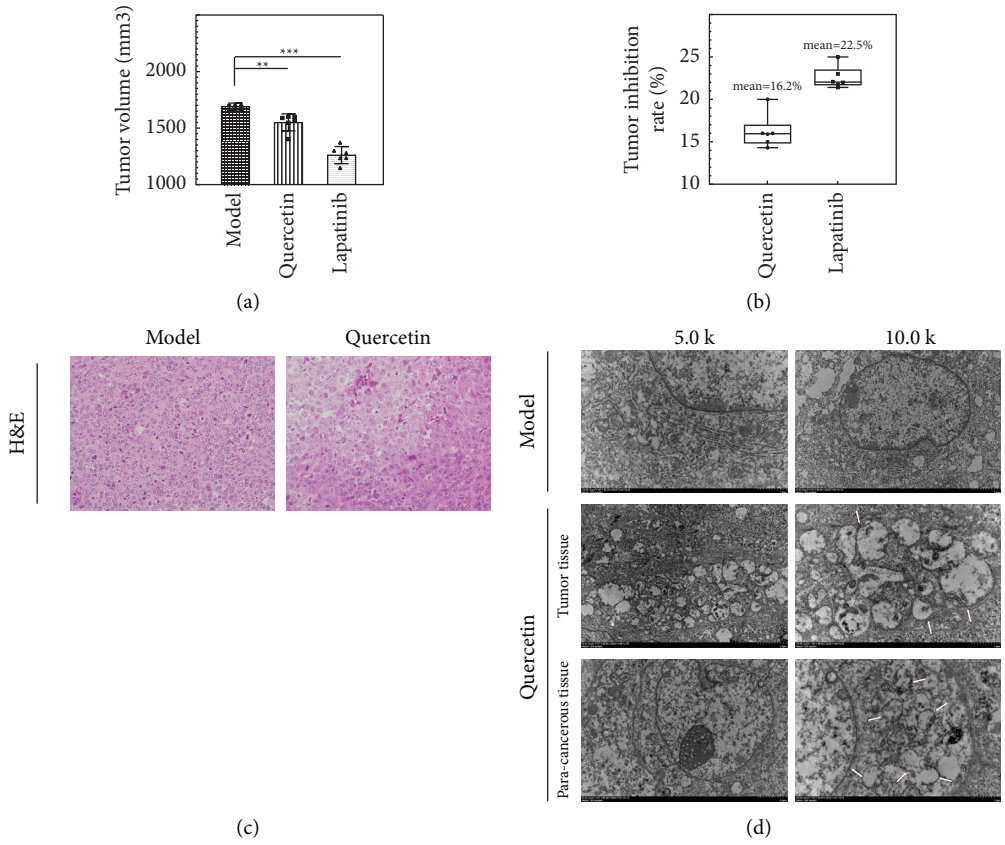

Figure 6: Continued.

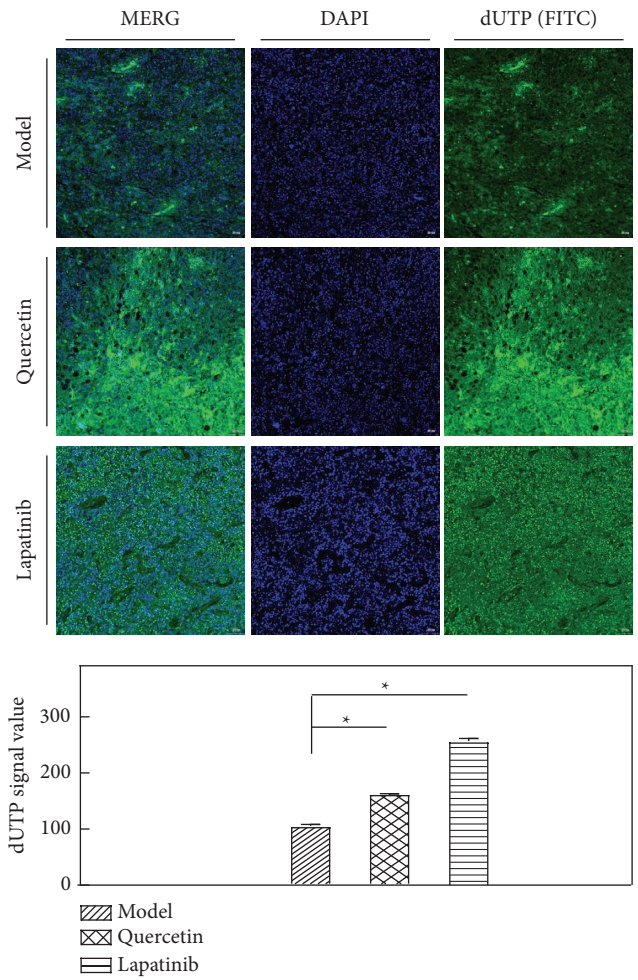

(e)

Figure 6: Continued.

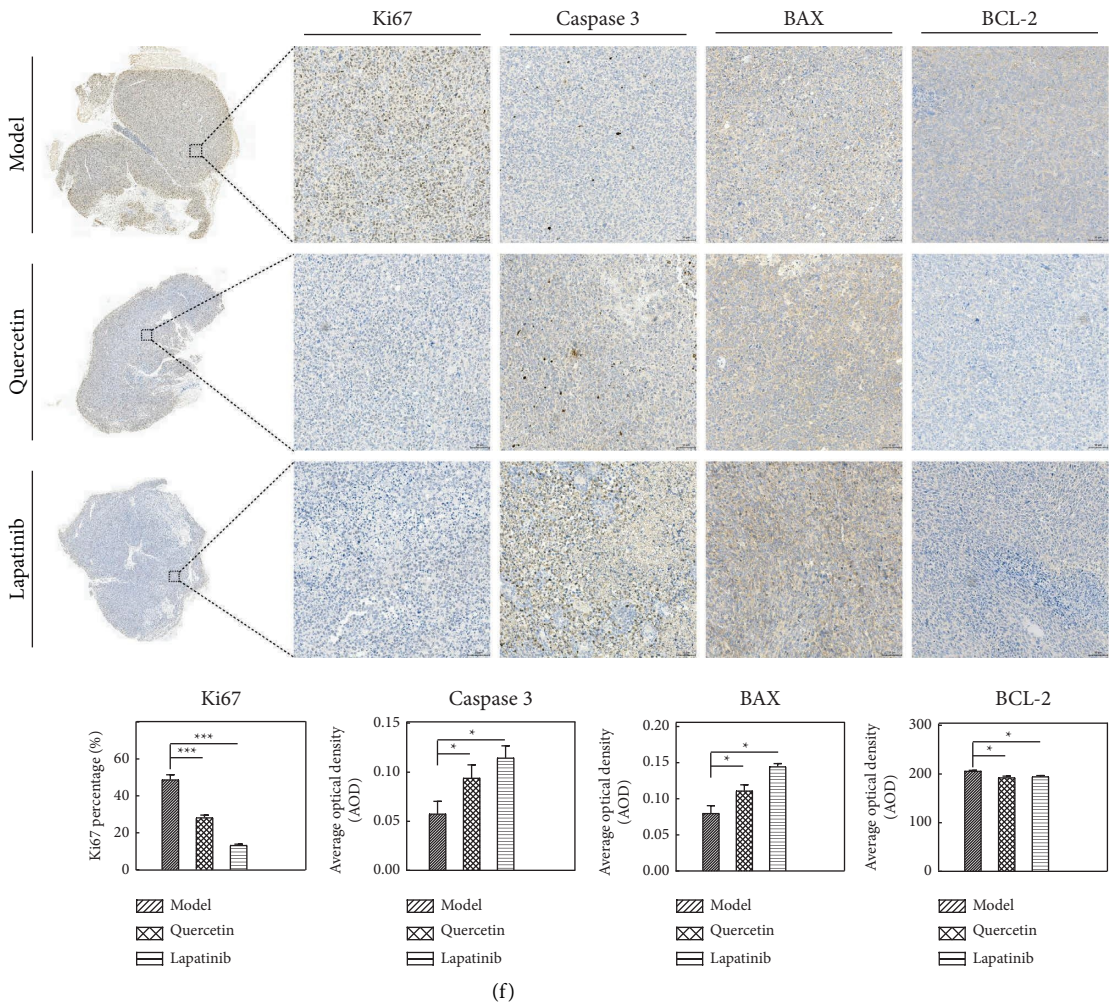

Figure 6: Quercetin treatment inhibits tumor growth in vivo. (a) The tumor volume. (b) The tumor inhibition rate. (c) H&E staining. (d) The mitochondrial damage (transmission electron microscopy). (e) The TUNEL assay. (f) Immunohistochemistry of Ki67, caspase 3, BAX, and BCL-2. $^{*}p < 0.05$ indicates differences between two groups; $^{**}p < 0.01$ was considered to be a significant difference; $^{***}p < 0.001$ was considered to be a highly significant difference.

also showed antitumor effects and exhibited multitarget and multipathway antitumor characteristics. Quercetin can generate high levels of ROS [13], inhibit inflammation [14], inhibit angiogenesis [15], induce tumor cell apoptosis [16], cause cell cycle arrest [17], and cause mitochondrial membrane potential loss [18]. Quercetin inhibits tumor growth through the PI3K/Akt and PTEN/Akt signaling pathways [19], STAT3/5 signaling cascade [20], and ERK1/2 and P38-MAPK signaling pathways [21].

In this study, after quercetin treatment, MKN-45 cells proliferated slowly, and the proportion of "S + G2M stage" cells decreased, causing cell cycle arrest. The cell apoptosis of MKN-45 also increased significantly, accompanied by increased Cyt-C, decreased BCL-2, decreased mitochondrial membrane potential, mitochondrial swelling, and ridge fractures.

Therefore, we speculated that mitochondria-mediated endogenous apoptosis is one of the mechanisms by which quercetin inhibits gastric cancer. The results of network pharmacology and molecular docking indicated that the EGFR and ERK/MAPK signaling pathways may play an important role in the action of quercetin against gastric cancer. To test these hypotheses, we detected key molecules of the ERK/MAPK signaling pathway and found that p-ERK1, p-MEK1, and PTGS2 levels decreased after quercetin treatment.

In addition, TBHQ (an ERK agonist) effectively inhibited quercetin-induced accelerated apoptosis and slowed cell proliferation. This suggests that quercetin targets EGFR, blocks the ERK signaling pathway, and down-regulates PTGS2 expression. In the in vivo experiments, after quercetin treatment, tumor volume was significantly reduced. Ki67 and BCL-2 levels in tumor tissue were decreased, caspase 3 and BAX were significantly increased, and mitochondrial damage was obvious. In summary, our study showed that quercetin has a good anticancer effect both in vivo and in vitro. It binds to EGFR in gastric cancer cells and inhibits tumor growth via the ERK signaling pathway.

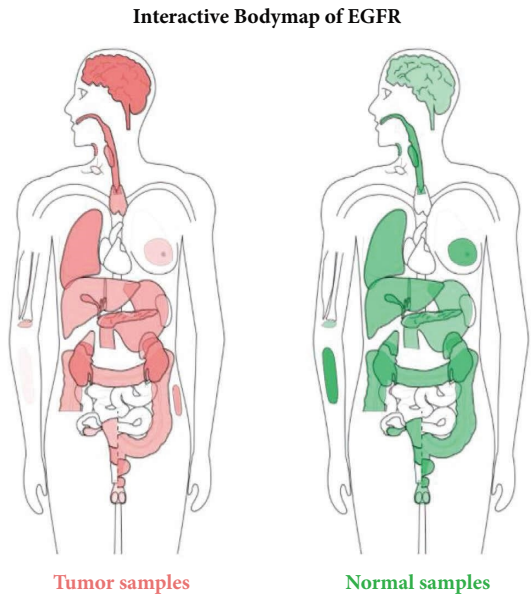

The median expression of tumor and normal samples in bodymap

Parts of the body	Tumor samples	Normal samples
Brain	6.38	2.32
Esophagus	5.3	4.42
Thyroid	4	4.13
Lymphonodus	0.58	0.03
Thymus	3.73	0.03
Blood	0.03	0.06
Lung	4.91	4.06
Breast	2.01	4.71
Stomach	3.82	2.88
Liver	3.32	3.72
Pancreas	3.38	2.59
Kidney	5.31	3.6
Adrenal Gland	2.35	3.5
Colon	3.31	3.61
Uterus	2.9	3.96
Cervix Uteri	4.23	4.29
Bladder	3.72	4.11
Testis	1.4	2.4
Prostate	3.76	4.3
Ovary	2.23	3.63
Synovial	3.27	2.67
Forearm	0.6	5.8
Neck	5.28	4.55
Abdomen	4.2	0
Cholangio	3.61	3.51

(a)

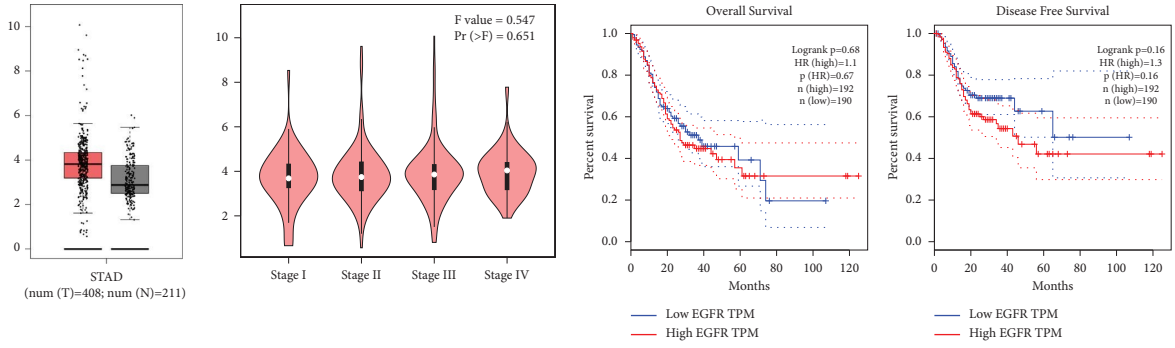

(b) (c) (d)

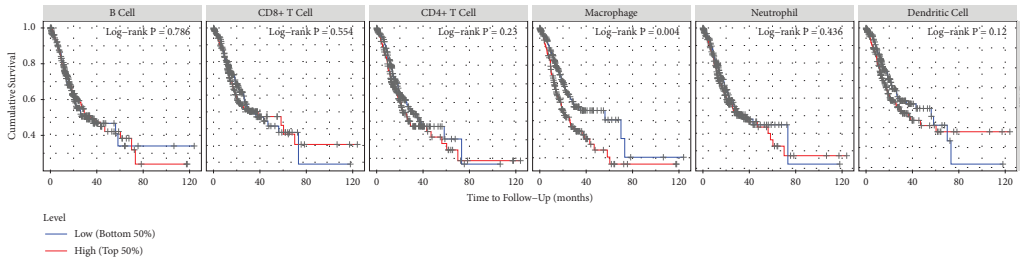

(e)

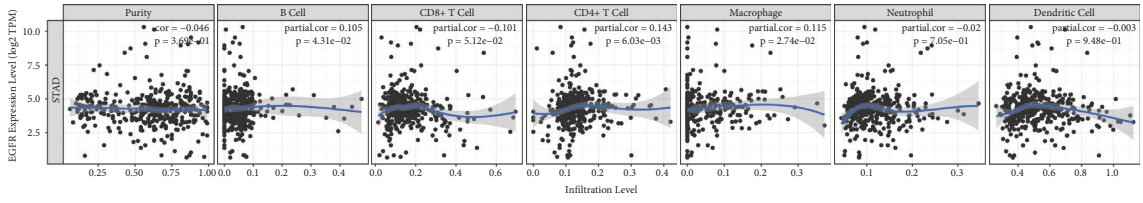

(f)

FIGURE 7: Prognostic value of EGFR and its correlation with tumor immune infiltration level. (a) Interactive body map in the GEPIA database. (b) The expression difference of EGFR in gastric cancer tissue and normal tissue (red: tumor tissue; green and black: normal tissue). (c) Correlation between EGFR and tumor stage in gastric cancer patients. (d) The prognostic value of EGFR in gastric cancer patients. (e) The relationship between the tumor immune infiltration level and cumulative survival. (f) The relationship between the tumor immune infiltration level and EGFR. $^{*}p < 0.05$ indicates differences between two groups; $^{**}p < 0.01$ was considered to be a significant difference; $^{***}p < 0.001$ was considered to be a highly significant difference.

Thus, it is expected to be a novel small-molecule inhibitor of EGFR.

EGFR plays an important role in tumor growth, invasion, metastasis, and neovascularization. It is overexpressed in various tumors, including gastric cancer [22]. In this study, correlation analysis between EGFR and gastric cancer or immune cell infiltration was performed using the GEPIA and TIMER databases. We found that EGFR was highly expressed in 12 human tumors, including gastric cancer (Figures 7(a) and 7(b)). However, there was no significant difference in EGFR expression between the different tumor stages (Figure 7(c)), and patients with low EGFR expression had a better OS ($p < 0.05$) and DFS than those with higher expression (Figure 7(d)). Immune cell infiltration in the tumor microenvironment can regulate tumorigenesis and tumor progression, further affecting patient prognosis. We found that the expression levels of EGFR were positively correlated with macrophages ($r > 0$, $p < 0.05$) and patients with low levels of macrophages had a better prognosis ($p < 0.05$; Figures 7(e) and 7(f)). These results indicated that an increase in EGFR was correlated with an increase in macrophages, which ultimately led to poor prognosis in patients with gastric cancer.

In recent years, EGFR is a common drug target for cancer treatment. Gefitinib and erlotinib are first-generation EGFR-tyrosine kinase inhibitors (EGFR-TKIs) approved by the Food and Drug Administration [23]. Second-generation EGFR-TKIs (afatinib, neratinib, canertinib, pelitinib, and dacomitinib [24, 25]) provide a sustained blocking effect on the basis of first-generation EGFR-TKIs, thus enhancing the lasting inhibition of tumor cells. Unfortunately, however, patients treated with EGFR-TKIs often develop antitumor resistance months after treatment, which is usually due to EGFR mutations and chemical resistance [26]. To overcome this obstacle, EGFR-TKIs targeting drug-resistant EGFR mutations have emerged. In 2022, the third-generation EGFR-TKI, ocitinib, was designated as a first-line anticancer drug [27, 28]. However, approximately 1-2 years after treatment, most patients showed disease progression, indicating that a new resistant phenotype has emerged. Recent studies have shown that EAI001/045 and JBJ-04-125-02 (fourth-generation EGFR-TKIs) can overcome EGFR L858R/T790M/C797S mutations and are highly selective for drug-resistant EGFR mutations. However, they are also unable to suppress del19/T790M/C797S [29, 30]. In summary, EGFR-TKIs have achieved good efficacy in cancer treatment; however, as with other macromolecular antibody drugs, new EGFR mutations and other resistance mechanisms appear rapidly after treatment. Moreover, they are expensive, which limits their clinical application.

Compared with monoclonal antibody drugs, quercetin is a natural small-molecule compound extracted from TCM and has the advantages of better cell permeability, short half-life, and low production cost. Our study showed that quercetin first targets EGFR, inhibits cell proliferation, and promotes apoptosis of gastric cancer cells through the ERK/MAPK signaling pathway.

The MAPK signaling pathway is associated with the occurrence and development of tumors [31–33]. The ERK signaling pathway is a branch of the MAPK signaling pathway, and its abnormal activation can lead to the acceleration of malignant transformation and abnormal proliferation of cancer cells [34]. PTGS2 is an important inflammatory factor downstream of the ERK/MAPK signaling pathway [35] and is mainly involved in cell proliferation, apoptosis, and other pathological and inflammatory reactions [36]. Therefore, blocking the activation of the ERK/MAPK signaling pathway and downregulating PTGS2 levels may be an effective way to inhibit tumor growth.

Our study demonstrated that quercetin plays an antitumor role by modulating the EGFR-ERK/MAPK signaling pathway and downregulating PTGS2. This is similar to that observed with other antitumor drugs. For example, periplocan [37], cathepsin S [38], 20 (S)-PPD [39], and gefitinib [40] also inhibit proliferation and promote apoptosis in cancer cells by blocking the EGFR-ERK/MAPK signaling pathway. An anti-LeY antibody enhances the effect of celecoxib by downregulating the MAPK/PTGS2 signaling pathway in gastric cancer [41]. Kaempferol effectively inhibits 6-hydroxydopamine-induced inflammatory damage in rat adrenal pheochromocytoma PC12 cells, which is associated with decreased PTGS2 levels after the inhibition of the p38-MAPK signaling pathway [42]. In liver cancer HepG2 cells, artesunate inhibits TNFA-induced MAPK signaling pathway activation, downregulates PTGS2 expression, and plays an anti-inflammatory role [43]. NS-398 (a PTGS2 inhibitor) targets MAPK (ERK2) kinase and significantly inhibits nonsteroidal anti-inflammatory drug-induced proliferation and growth of MKN-28 cells [44]. Tanshinone IIA can effectively reduce the inflammatory response induced by *Helicobacter pylori* infection through the NF-kB and MAPK pathways, reduce PTGS2 levels, and promote endogenous apoptosis [45]. Finally, the MEK1/2 inhibitor PD0325901 blocked the ERK pathway (by decreasing pERK levels) and PTGS2 expression in gastric cancer SGC7901 cells [46].

5. Conclusions

In conclusion, our study showed that quercetin binds to EGFR in gastric cancer cells and promotes mitochondria-mediated endogenous apoptosis by blocking the ERK/MAPK signaling pathway. At the same time, quercetin has the advantages of a short half-life, high oral availability, and low price and is expected to become a novel natural small-molecule EGFR inhibitor. This study provides a theoretical basis for licorice against gastric cancer, new targets for the evaluation of clinical efficacy, and a new direction for exploring the potential mechanisms underlying the antitumor

activity of licorice. However, tumor heterogeneity and genomic instability are the biological characteristics of tumors. The antitumor effect of TCM involves multiple components, targets, and pathways. Therefore, further investigation is warranted to determine whether quercetin induces drug resistance. In future studies, we aim to explore the underlying mechanisms of action of licorice against gastric cancer.

Data Availability

The data used to support the findings of this study are available from the corresponding author upon reasonable request.

Additional Points

Practical Applications. The mechanism of action of quercetin against gastric cancer may involve blocking the EGFR-ERK signaling pathway and promoting mitochondria-mediated endogenous apoptosis. This study proves that quercetin is a novel EGFR small-molecule inhibitor and also provides a theoretical basis for quercetin in the treatment of gastric cancer.

Conflicts of Interest

The authors declare that they have no conflicts of interest.

Authors' Contributions

Yali Liu conceptualized the study, proposed the methodology, investigated the study, reviewed and edited the manuscript, and performed funding acquisition and in vitro and in vivo experiments. Yong Zhang conceptualized and supervised the study. Qiaoying Jin conceptualized and investigated study and reviewed and edited the manuscript. Yan Li validated the study and performed formal analysis. Xin Zheng performed data curation and supervised the study. Yanjun Jiang and Tianming Wang visualized the study, provided the software, and performed data curation. Jing Li, Biyun Zhang, and Jiarui Zhu performed in vitro experiment and data curation. Xintong Wei and Ruihua Huang performed in vivo experiments and data curation.

Acknowledgments

We would like to give our heartfelt thanks to the Cuiying Biomedical Research Center, Lanzhou University Second Hospital. This research was funded by the Lanzhou Science and Technology Plan Program (grant number 2023-4-30), the Cuiying Scientific and Technological Innovation Program of Lanzhou University Second Hospital (grant numbers CY2019-QN13 and CY2017-QN19), the Innovation Fund for Higher Education of Gansu Province (grant numbers 2020B-038, 2021B-041, and 2022B-051), and the Cuiying Scientific Training Program for Undergraduates of Lanzhou University Second Hospital (grant numbers CYXZ2023-22 and CYXZ2023-31).

References

[1] H. Sung, J. Ferlay, R. L. Siegel et al., "Global cancer statistics 2020: GLOBOCAN estimates of incidence and mortality worldwide for 36 cancers in 185 countries," *CA: A Cancer Journal for Clinicians*, vol. 71, no. 3, pp. 209–249, 2021.

[2] M. Bala, S. Kumar, K. Pratap, P. K. Verma, Y. Padwad, and B. Singh, "Bioactive isoquinoline alkaloids from Cissampelos pareira," *Natural Product Research*, vol. 33, no. 5, pp. 622–627, 2019.

[3] M. Bala, K. Pratap, P. K. Verma, B. Singh, and Y. Padwad, "Validation of ethnomedicinal potential of Tinospora cordifolia for anticancer and immunomodulatory activities and quantification of bioactive molecules by HPTLC," *Journal of Ethnopharmacology*, vol. 175, pp. 131–137, 2015.

[4] M. Greenwell and P. K. Rahman, "Medicinal plants: their use in anticancer treatment," *International Journal of Pharmaceutical Sciences and Research*, vol. 6, no. 10, pp. 4103–4112, 2015.

[5] S. Kauroo, J. Govinden-Soulange, V. M. Ranghoo-Sanmukhiya et al., "Extracts of select endemic plants from the Republic of Mauritius exhibiting anti-cancer and immunomodulatory properties," *Scientific Reports*, vol. 11, no. 1, p. 4272, 2021.

[6] A. Kumar, S. Kaur, S. Dhiman et al., "Targeting Akt/NF-κB/p53 pathway and apoptosis inducing potential of 1,2-benzenedicarboxylic acid, bis (2-methyl propyl) ester isolated from Onosma bracteata Wall. against human osteosarcoma (MG-63) cells," *Molecules*, vol. 27, no. 11, p. 3478, 2022.

[7] B. R. Huck, L. Kötzner, and K. Urbahns, "Small molecules drive big improvements in immuno-oncology therapies," *Angewandte Chemie International Edition*, vol. 57, no. 16, pp. 4412–4428, 2018.

[8] H. Wang, X. H. Ge, H. H. Qu et al., "Glycyrrhizic acid inhibits proliferation of gastric cancer cells by inducing cell cycle arrest and apoptosis," *Cancer Management and Research*, vol. 12, pp. 2853–2861, 2020.

[9] X. Lin, Y. H. Chen, P. P. Wang, C. X. Wang, and X. L. Li, "Effects of flavonoid components on other drugs in Chinese medicine and Food Homology mediated by Metabolic enzymes and transporters," *China Pharmacy*, vol. 32, no. 18, pp. 2287–2293, 2021.

[10] W. J. Hao, X. Yuan, L. N. Yu et al., "Licochalcone A-induced human gastric cancer BGC-823 cells apoptosis by regulating ROS-mediated MAPKs and PI3K/AKT signaling pathways," *Scientific Reports*, vol. 5, no. 1, Article ID 10336, 2015.

[11] X. R. Zhang, S. Y. Wang, W. Sun, and C. Wei, "Isoliquiritigenin inhibits proliferation and metastasis of MKN28 gastric cancer cells by suppressing the PI3K/AKT/mTOR signaling pathway," *Molecular Medicine Reports*, vol. 18, no. 3, pp. 3429–3436, 2018.

[12] F. Zhang, *Functions and Mechanisms of ZNF165 in Gastric Cancer*, Lanzhou University, Lanzhou, China, 2022.

[13] A. Sheik, K. Kim, G. L. Varaprasad et al., "The anti-cancerous activity of adaptogenic herb Astragalus membranaceus," *Phytomedicine*, vol. 91, Article ID 153698, 2021.

[14] Y. Li, J. Y. Yao, C. Y. Han et al., "Quercetin, inflammation and immunity," *Nutrients*, vol. 8, no. 3, p. 167, 2016.

[15] G. Lupo, M. T. Cambria, M. Olivieri et al., "Anti-angiogenic effect of quercetin and its 8-methyl pentamethyl ether derivative in human microvascular endothelial cells," *Journal of Cellular and Molecular Medicine*, vol. 23, no. 10, pp. 6565–6577, 2019.

[16] X. Shen, Y. Si, Z. Wang, J. Wang, Y. Guo, and X. Zhang, "Quercetin inhibits the growth of human gastric cancer stem cells by inducing mitochondrial-dependent apoptosis through the inhibition of PI3K/Akt signaling," *International Journal of Molecular Medicine*, vol. 38, no. 2, pp. 619–626, 2016.

[17] Y. S. Ma, C. N. Yao, H. C. Liu et al., "Quercetin induced apoptosis of human oral cancer SAS cells through mitochondria and endoplasmic reticulum mediated signaling pathways," *Oncology Letters*, vol. 15, no. 6, pp. 9663–9672, 2018.

[18] H. Liu and M. Zhou, "Antitumor effect of quercetin on Y79 retinoblastoma cells via activation of JNK and p38 MAPK pathways," *BMC Complementary and Alternative Medicine*, vol. 17, no. 1, p. 531, 2017.

[19] A. Rauf, M. Imran, I. A. Khan et al., "Anticancer potential of quercetin: a comprehensive review," *Phytotherapy Research*, vol. 32, no. 11, pp. 2109–2130, 2018.

[20] H. S. Seo, J. M. Ku, H. S. Choi et al., "Quercetin induces caspase-dependent extrinsic apoptosis through inhibition of signal transducer and activator of transcription 3 signaling in HER2-overexpressing BT-474 breast cancer cells," *Oncology Reports*, vol. 36, no. 1, pp. 31–42, 2016.

[21] H. Li and C. Chen, "Quercetin has antimetastatic effects on gastric cancer cells via the interruption of uPA/uPAR function by modulating NF-κB, PKC-δ, ERK1/2, and AMPKα," *Integrative Cancer Therapies*, vol. 17, no. 2, pp. 511–523, 2018.

[22] G. H. Shan, F. Hua, T. Chen, and S. Han, "Expression of cyclooxygenase-2 and epidermal growth factor receptor in gastric cancer and precancerous lesions and its relationship with *Helicobacter pylori* infection," *Journal of Hunan University Natural Sciences*, vol. 5, pp. 67–70, 2019.

[23] Y. Liu, Y. Zhang, G. Feng et al., "Comparison of effectiveness and adverse effects of gefitinib, erlotinib and icotinib among patients with non-small cell lung cancer: a network meta-analysis," *Experimental and Therapeutic Medicine*, vol. 14, no. 5, pp. 4017–4032, 2017.

[24] Z. Yang, A. Hackshaw, Q. Feng et al., "Comparison of gefitinib, erlotinib and afatinib in non-small cell lung cancer: a meta-analysis," *International Journal of Cancer*, vol. 140, no. 12, pp. 2805–2819, 2017.

[25] T. S. Mok, Y. Cheng, X. Zhou et al., "Updated overall survival in a randomized study comparing dacomitinib with gefitinib as first-line treatment in patients with advanced non-small-cell lung cancer and EGFR-activating mutations," *Drugs*, vol. 81, no. 2, pp. 257–266, 2021.

[26] L. Porcelli, E. Giovannetti, Y. G. Assaraf et al., "The EGFR pathway regulates BCRP expression in NSCLC cells: role of erlotinib," *Current Drug Targets*, vol. 15, no. 14, pp. 1322–1330, 2014.

[27] D. S. Ettinger, D. E. Wood, D. L. Aisner et al., "NCCN guidelines insights: non-small cell lung cancer version 2.2021," *Journal of the National Comprehensive Cancer Network*, vol. 19, no. 3, pp. 254–266, 2021.

[28] M. Singhal, M. Walia, and M. S. Kamle, "Ideal sequencing in Stage IV epidermal growth factor receptor mutant non-small-Cell Lung Cancer," *Indian Journal of Cancer*, vol. 59, no. 5, p. 80, 2022.

[29] C. To, J. Jang, T. Chen et al., "Single and dual targeting of mutant EGFR with an allosteric inhibitor," *Cancer Discovery*, vol. 9, no. 7, pp. 926–943, 2019.

[30] Y. Jia, C. H. Yun, E. Park et al., "Overcoming EGFR(T790M) and EGFR(C797S) resistance with mutant-selective allosteric inhibitors," *Nature*, vol. 534, no. 7605, pp. 129–132, 2016.

[31] H. Liu, S. H. Shin, H. Chen et al., "CDK12 and PAK2 as novel therapeutic targets for human gastric cancer," *Theranostics*, vol. 10, no. 14, pp. 6201–6215, 2020.

[32] J. Du, Y. Liang, J. Li, J. M. Zhao, and X. Y. Lin, "LINC00858 knockdown inhibits gastric cancer cell growth and induces apoptosis through reducing WNK2 promoter methylation," *Cellular Oncology*, vol. 44, no. 1, p. 235, 2021.

[33] B. Xu, S. Li, Y. Fang et al., "Proprotein convertase subtilisin/Kexin Type 9 promotes gastric cancer metastasis and suppresses apoptosis by facilitating MAPK signaling pathway through HSP70 up-regulation," *Frontiers in Oncology*, vol. 10, Article ID 609663, 2020.

[34] Y. Q. Hao and H. X. Zheng, "Study on the mechanism of MAPK/ERK signaling pathway in tumor therapy," *China Journal of Leprosy and Skin Diseases*, vol. 28, no. 7, pp. 490–493, 2012.

[35] X. P. Zhu, X. Ren, R. Li, D. Yu, and Y. M. Kang, "Inhibitory effects of nonsteroidal anti-inflammatory drugs celecoxib and indomethacin on gastric cancer cells MKN45," *The Journal of Pathology: Clinical Research*, vol. 39, no. 4, pp. 714–720, 2019.

[36] X. Wang, Z. L. Yu, C. Wang et al., "Alantolactone, a natural sesquiterpene lactone, has potent antitumor activity against glioblastoma by targeting IKKβ kinase activity and interrupting NF-κB/COX-2-mediated signaling cascades," *Journal of Experimental and Clinical Cancer Research*, vol. 36, no. 1, p. 93, 2017.

[37] H. Ye, X. Wei, C. Meng et al., "Mechanism of action of periplogenin on nasopharyngeal carcinoma based on network pharmacology and experimental study of vitamin E coupled with periplogenin self-assembled nano-prodrug for nasopharyngeal carcinoma," *Journal of Biomedical Nanotechnology*, vol. 16, no. 9, pp. 1406–1415, 2020.

[38] K. L. Chen, W. S. Chang, C. H. Cheung et al., "Targeting cathepsin S induces tumor cell autophagy via the EGFR-ERK signaling pathway," *Cancer Letters*, vol. 317, no. 1, pp. 89–98, 2012.

[39] T. Zhang, Y. Liang, P. Zuo et al., "20(S)-Protopanaxadiol blocks cell cycle progression by targeting epidermal growth factor receptor," *Food and Chemical Toxicology*, vol. 135, Article ID 111017, 2020.

[40] X. S. Bai, *RNF128 Promotes the Invasion and Metastasis of Hepatocellular Carcinoma via EGFR/MEK/ERK Signaling Pathway*, Dalian Medical University, Dalian, China, 2021.

[41] F. Aziz, I. Khan, S. Shukla et al., "Partners in crime: the lewis y antigen and fucosyltransferase iv in helicobacter pylori-induced gastric cancer," *Pharmacology and Therapeutics*, vol. 232, Article ID 107994, 2022.

[42] M. Y. Cai, W. X. Zhuang, E. Lyu, and W. Y. Fu, "Kaempferol attenuates 6-OHDA-induced inflammatory damage in PC12 cells via inhibting p38 MAPK signaling pathway," *Chinese Journal of Cellular and Molecular Immunology*, vol. 36, no. 7, pp. 583–589, 2020.

[43] Q. Zhang, *The Experimental Study of Artesunate on TNFα-Induced Inflammatory Response of Hep G2 Cells by Regulating the MAPK/NF-kB Signaling Pathways*, Yanbian University, Jilin, China, 2018.

[44] S. S. Husain, I. L. Szabo, R. Pai et al., "MAPK (ERK2) kinase—a key target for NSAIDs-induced inhibition of gastric cancer cell proliferation and growth," *Life Sciences*, vol. 69, no. 25–26, pp. 3045–3054, 2001.

[45] G. Y. Chen, Y. C. Shu, D. Y. Chuang, and Y. C. Wang, "Inflammatory and apoptotic regulatory activity of tanshinone IIA in Helicobacter pylori-infected cells," *The American Journal of Chinese Medicine*, vol. 44, no. 06, pp. 1187–1206, 2016.

[46] Y. F. Qi, *EBV Down-Regulates COX-2 Expression via TRAF2 and ERK Signal Pathway in EBV-Associated Gastric Cancer*, Qingdao University, Qingdao, China, 2020.